Bioorg. Med. Chem. 42 (2021) 116266

Contents lists available at ScienceDirect

Bioorganic & Medicinal Chemistry

journal homepage: www.elsevier.com/locate/bmc

From triazolophthalazines to triazoloquinazolines: A bioisosterism-guided approach toward the identification of novel PCAF inhibitors with potential anticancer activity

Mohamed H. El-Shershaby [a], Adel Ghiaty [a], Ashraf H. Bayoumi [a], Ahmed A. Al-Karmalawy [b], Ebtehal M. Husseiny [c], Mona S. El-Zoghbi [d], Hamada S. Abulkhair [a,b,*]

[a] Pharmaceutical Organic Chemistry Department, Faculty of Pharmacy (Boys), Al-Azhar University, Nasr City 11884, Cairo, Egypt
[b] Pharmaceutical Chemistry Department, Faculty of Pharmacy, Horus University – Egypt, International Coastal Road, 34518 New Damietta, Egypt
[c] Department of Pharmaceutical Organic Chemistry, Faculty of Pharmacy (Girls), Al-Azhar University, Nasr City, Cairo, Egypt
[d] Pharmaceutical Chemistry Department, Faculty of Pharmacy, Menoufia University, Gamal Abd El-Nasir Street, Shebin El-Koum, Egypt

ARTICLE INFO

Keywords:
Anticancer
PCAF
Bioisosterism
Synthesis
Triazoloquinazoline
Apoptosis

ABSTRACT

Inhibition of PCAF bromodomain has been validated as a promising strategy for the treatment of cancer. In this study, we report the bioisosteric modification of the first reported potent PCAF bromodomain inhibitor, L-45 to its triazoloquinazoline bioisosteres. Accordingly, three new series of triazoloquinazoline derivatives were designed, synthesized, and assessed for their anticancer activity against a panel of four human cancer cells. Three derivatives demonstrated comparable cytotoxic activity with the reference drug doxorubicin. Among them, compound **22** showed the most potent activity with IC_{50} values of 15.07, 9.86, 5.75, and 10.79 μM against Hep-G2, MCF-7, PC3, and HCT-116 respectively. Also, compound **24** exhibited remarkable cytotoxicity effects against the selected cancer cell lines with IC_{50} values of 20.49, 12.56, 17.18, and 11.50 μM. Compounds **22** and **25** were the most potent PCAF inhibitors (IC_{50}, 2.88 and 3.19 μM, respectively) compared with bromosporine (IC_{50}, 2.10 μM). Follow up apoptosis induction and cell cycle analysis studies revealed that the bioisostere **22** could induce apoptotic cell death and arrest the cell cycle of PC3 at the G2/M phase. The *in silico* molecular docking studies were additionally performed to rationalize the PCAF inhibitory effects of new triazoloquinazoline bioisosteres.

1. Introduction

Histone acetyltransferase paralogues p300/CBP-associated factor (PCAF, EC 2.3.1.48) is one member belonging to the subfamily I of the phylogenetic bromodomain tree [1,2]. Mis-regulation of PCAF has been shown to be linked to abnormal cell proliferation and carcinogenesis [3–5]. Therefore, PCAF has emerged as an interesting target for the development of anticancer chemotherapeutics [2,6,7].

Quinazolines are a group of nitrogen-containing heterocyclic compounds that have gained particular importance as they featured in many FDA-approved anticancer agents [8] (Fig. 1). These include gefitinib (**1**; Iressa®), vandetanib (**2**; Caprelsa®), erlotinib (**3;** Tarceva®), lapatinib (**4**; Tykreb®), afatinib (**5**; Gilotrif®), and dacomitinib (**6**; Vizimpro®). Soon after, on April 2020, tucatinib (**7;** Tukysa®) was the last FDA-approved quinazoline as an anticancer molecule. Tucatinib is used for the treatment of adult patients with advanced metastatic breast cancer, including patients with brain metastases [9].

Both the quinazoline [10–12] and 1,2,4-triazole [13–17] heterocycles have individually studied in many articles as interesting classes of anticancer drugs. Although, the investigation of 1,2,4-triazoloquinazolines as anticancer has reported in few articles. To the best of our knowledge, six attempts were done for the development of triazoloquinazoline derivatives with antitumor activity (Fig. 2) [18–23]. Among these, two articles studied the anticancer activity of [1,2,4]triazolo[1,5-*c*]quinazolines [18,19]. The third one, reported the potent anticancer activity of [1,2,4]triazolo[4,3-*a*]quinazolin-5-one derivatives **8** and **9** against a panel of human cancer cell lines [20]. In 2014, the *in vitro* cytotoxicity of twenty two 1,2,4-Triazolo[1,5-*a*]quinazolines was evaluated against medulloblastoma, hepatocellular carcinoma, and melanoma cell lines [21]. The last two articles were published in the last year [22,23] and led to the discovery of new1,2,4-triazolo[4,3-*c*]quinazolines as a new class of DNA intercalators and potential inhibitors of both the EGFR-TK, and

* Corresponding author at: Pharmaceutical Organic Chemistry Department, Faculty of Pharmacy, Al-Azhar University, Nasr City 11884, Cairo, Egypt.
E-mail address: hamadaorganic@azhar.edu.eg (H.S. Abulkhair).

https://doi.org/10.1016/j.bmc.2021.116266
Received 8 April 2021; Received in revised form 29 May 2021; Accepted 31 May 2021
Available online 5 June 2021

topoisomerase II. These latter studies reported the EGFR inhibition activity of **13** and **14** with IC_{50} values ranging from 0.69 to 1.8 μM.

Few years ago, L-45 (**15,** Fig. 3) was identified as the first potent, highly selective, and cell-active PCAF bromodomain inhibitor belonging to the class of [1,2,4]triazolo[3,4-*a*]phthalazines [4]. Our recent couple of research articles reported the design and PCAF bromodomain inhibitory effects of certain triazolopthalazines as congeners of L-45 [15,23]. The PCAF antagonistic effects of L-45 was reported to be mediated through the formation of three key interactions with the binding site of histone acetyltransferase (Fig. 4): i) a hydrogen bonding interaction between the side chain NH functionality attached with C-6 of triazolophthalazine core and the Glu1389 residue; ii) a π-π stacking interaction between the pyridazine ring and the Tyr1442 residue; iii) an additional hydrogen bonding interaction between the *N*-1 of triazole ring and the Asn1436 residue. The present study aims to use the strategy of bioisosterism for the development of 1,2,4-triazolo[4,3-*c*]quinazolines congeners of L-45 as a suggested new scaffold of PCAF inhibitors. This bioisosteric transformation is expected to furnish new derivatives capable to interact with the PCAF receptor site in a similar pattern with that of the lead compound, L-45.

Bioisosterism is a key concept used by medicinal chemists for the modification of certain lead compounds to safer and more clinically useful agents. The crucial component for bioisosterism is that bioisosteres are expected to affect the same biological target without considerable perturbation in the biological activity [25]. As initially specified by Friedman, bioisosteres must include all atoms and molecules which fit the widest definition for isosteres and have a similar type of biological activity [26]. A more recent definition of bioisosteres has been broadened to include compounds or groups that retain nearly equal molecular shapes, volumes, and approximately the same distribution of electrons, which exhibit similar physicochemical properties.

1.1. Rationale and aim of the work

Considering the biological importance of 1,2,4-triazole and quinazoline rings as verified pharmacophores in FDA approved anticancer agents and as a continuation of our recent studies [27–30] of identifying new effective anticancer molecules, synthesis of three new sets of 1,2,4-triazolo[4,3-*c*]quinazoline derivatives, as bioisosteres of L-45, was carried out. The design of new compounds depended on the concept of bioisosterism as an interesting approach for the improvement of both the physicochemical properties and the biological activity. Meanwhile, we considered keeping the *N*-1 of the triazole ring in L-45 as an essential fragment that maintains the interaction with the essential amino acid residue Asn1436 in the target protein. Two bioisosteric modifications were adopted in the newly designed 1,2,4-triazolo[4,3-*c*]quinazolines (Fig. 5): i) The pyridazine ring of L-45 was replaced with its isosteric pyrimidine to keep the favorable π-π stacking interaction with the amino acid residue Tyr1442 in PCAF protein binding site; ii) The C-6 attached 1,2-ethylenediamine functionality of L-45 was replaced in two series with other fragments with different number and types of the HBD/HBA groups (series 1, 2). The significance of HBD/HBA groups at C-6 was investigated in the third series (series 3), *via* replacement with other fragments which have no ability of hydrogen bond formation. All the new compounds were evaluated for their *in vitro* anticancer activity against hepatocellular carcinoma (Hep-G2), mammary gland breast cancer (MCF-7), human prostate cancer (PC3), and colorectal carcinoma (HCT-116). In addition, follow up *in vitro* PCAF inhibition assay, apoptosis induction, and cell cycle analysis studies were conducted to evaluate the possible underlying anticancer mechanisms of the most active compounds. Furthermore, an *in silico* docking study was conducted to rationalize the ability of the designed bioisosteres to bind with the active site of histone acetyltransferase PCAF as a proposed mode of their anticancer activity. Finally, ADMET profiles of the best effective derivatives were evaluated to determine their potentials to build up as good drug candidates.

2. Results and discussion

2.1. Chemistry

The synthetic approach adopted for the synthesis of the starting triazoloquinazoline **20** is presented in Scheme 1**.** Briefly, a solution of potassium cyanate was added portion-wise into a solution of anthranilic acid in glacial acetic. The produced quinazoline-2,4(1*H*,3*H*)-dione treated with phosphorus oxychloride to get 2,4-dichloroquinazoline (**18**). The addition of hydrazine hydrate dropwise to the latter at 0–5 °C gives 2-chloro-4-hydrazinylquinazoline (**19**) [31,32], which was further treated with propionic anhydride [33,34] to obtain the desired starting 3-ethyl-[1,2,4]triazolo[4,3-*c*]quinazolin-5(6*H*)-one (**20**).

The structure of **20** was established based on its elemental and spectral data. The disappearance of the NH_2 biforked absorption band of the starting hydrazinyl derivative together with the appearance of a new amidic C═O absorption band at 1685 cm^{-1} in the IR spectrum confirmed the construction of the tricyclic ring. Also, the ^1H NMR

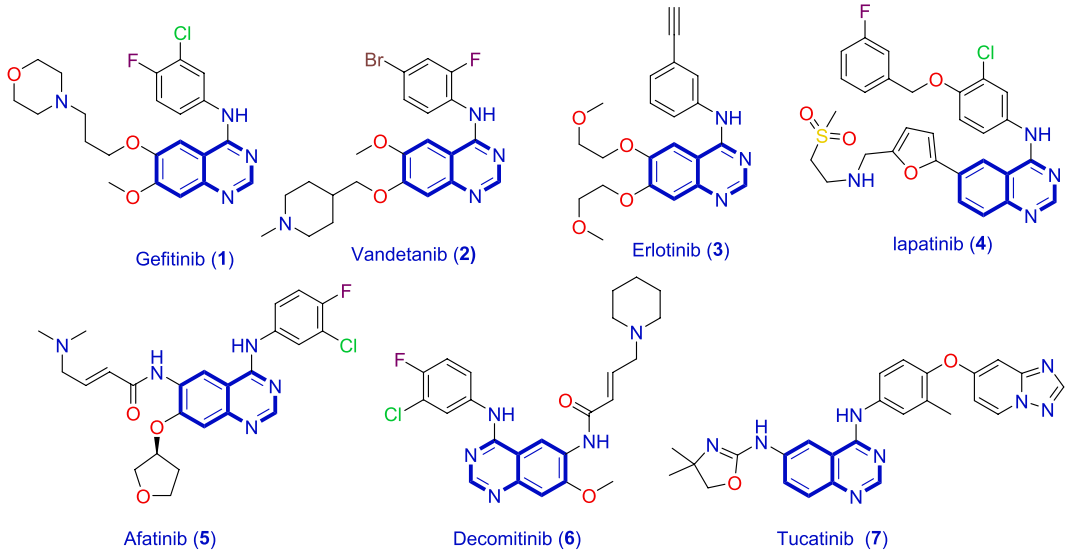

Fig. 1. Structures of quinazoline-derived FDA approved anticancer agents.

spectrum revealed a singlet signal at 12.28 ppm which is D_2O exchangeable due to the amidic NH. The ethyl group at C-3 presented quartet and triplet signals in the aliphatic region at 2.84 and 1.33 ppm. ^{13}C NMR spectrum of this compound revealed eleven carbon types, among which the carbonyl carbon exhibited its signal as expected at δ value of 167.83 ppm.

As represented in Scheme 2, our convergent synthesis approach of final target molecules **21**–**27** started by using a simple and straightforward strategy. The construction of this set of compounds began by reacting compound **20** with previously prepared α-chloro-*N*-arylacetamides [34–37]. The selected approach depended on the highly reliable and well-established electrophilic substitution reaction, exploiting the good commercial availability of aniline derivatives and chloroacetyl chloride precursors. Adopting this approach, seven 2-(3-ethyl-5-oxo-[1,2,4]triazolo[4,3-*c*]quinazolin-6(5*H*)-yl)-*N*-arylacetamide derivatives (**21**–**27**) were afforded in yields ranging from 68 to 86%. All the IR, ^1H NMR, ^{13}C NMR spectra of these amide derivatives were in accordance with assumed structures. In all compounds, the ^1H NMR spectra showed singlet signals of CH_2 fragments at the range of 4.45–4.06 ppm. The purity of synthesized compounds was monitored by TLC and confirmed by elemental analysis.

Next, to synthesize the ester derivatives of series 2 (**28**–**30**), a mixture of **20** and the appropriate alkyl chloroalkanoate was heated up to reflux in the presence of potassium carbonate to give the desired compound according to the reported procedure [27,38,39]. Adopting this approach, three ester derivatives were obtained in a satisfactory yield. All the IR, ^1H NMR, ^{13}C NMR spectra of these derivatives were consistent with expected structures. In all compounds, the ^1H NMR spectra showed singlet signals of N—CH_2C═O fragments around 5.0 ppm which appear deshielded by effects of both the nitrogen atom and the carbonyl group.

Afterward, to prepare the 6-alkyltriazoloquinazolinone derivatives of the third series (**31**–**35**), the starting 3-ethyl-[1,2,4]triazolo[4,3-*c*]quinazolin-5(6*H*)-one (**20**) was allowed to react with the appropriate alkyl halide in the presence of potassium carbonate according to the reported procedure [40]. Progress of all the chemical reactions were validated by TLC methodology and final products were purified by the

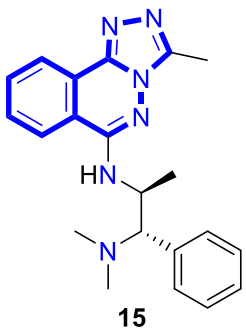

Fig. 3. L-45, the first potent and highly selective PCAF inhibitory triazolophthalazine.

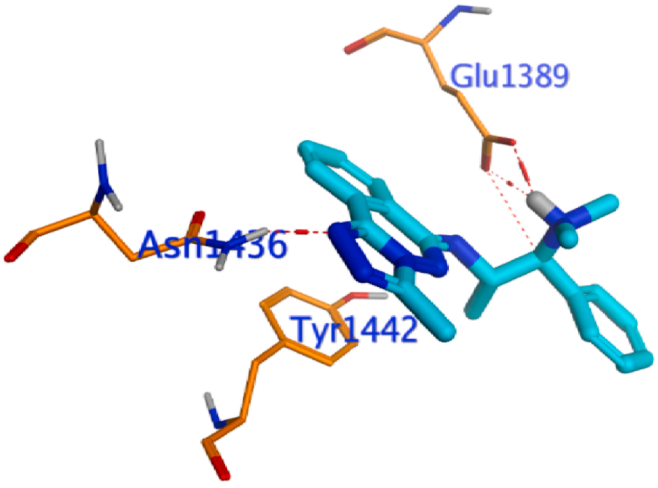

Fig. 4. The key interactions of L-45 (**15**) with the active site of PCAF.

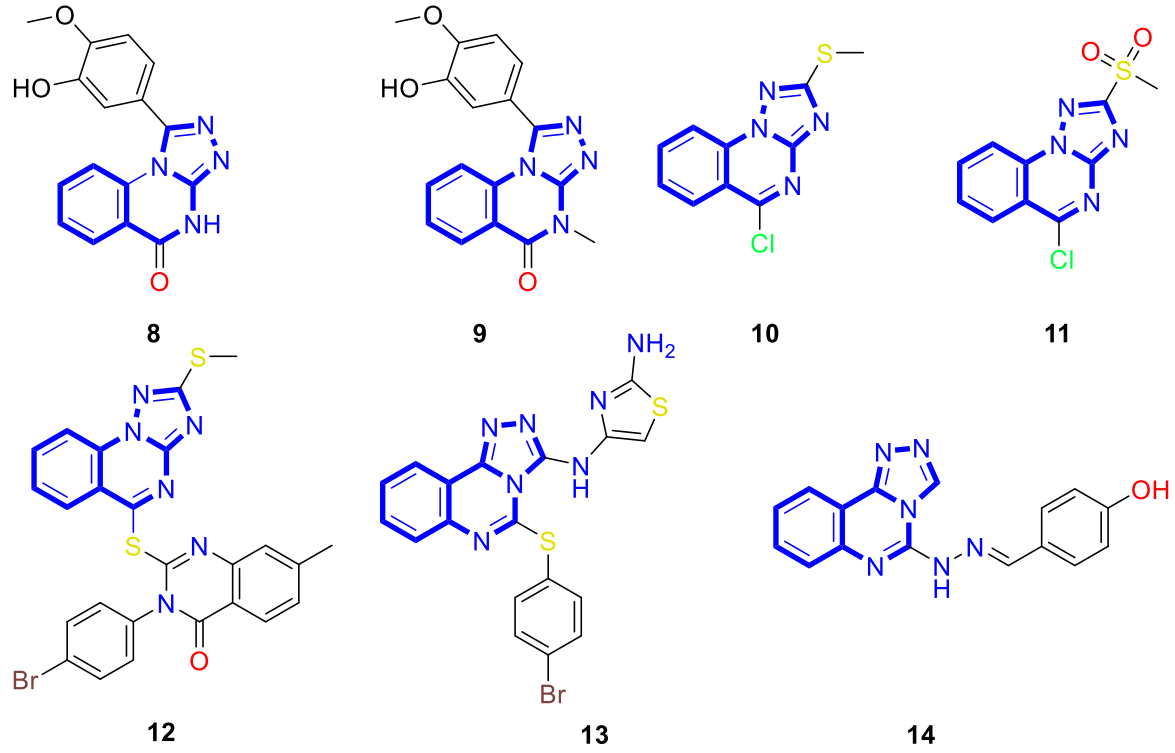

Fig. 2. Structures of selected [1,2,4]triazoloquinazines with potent anticancer activity.

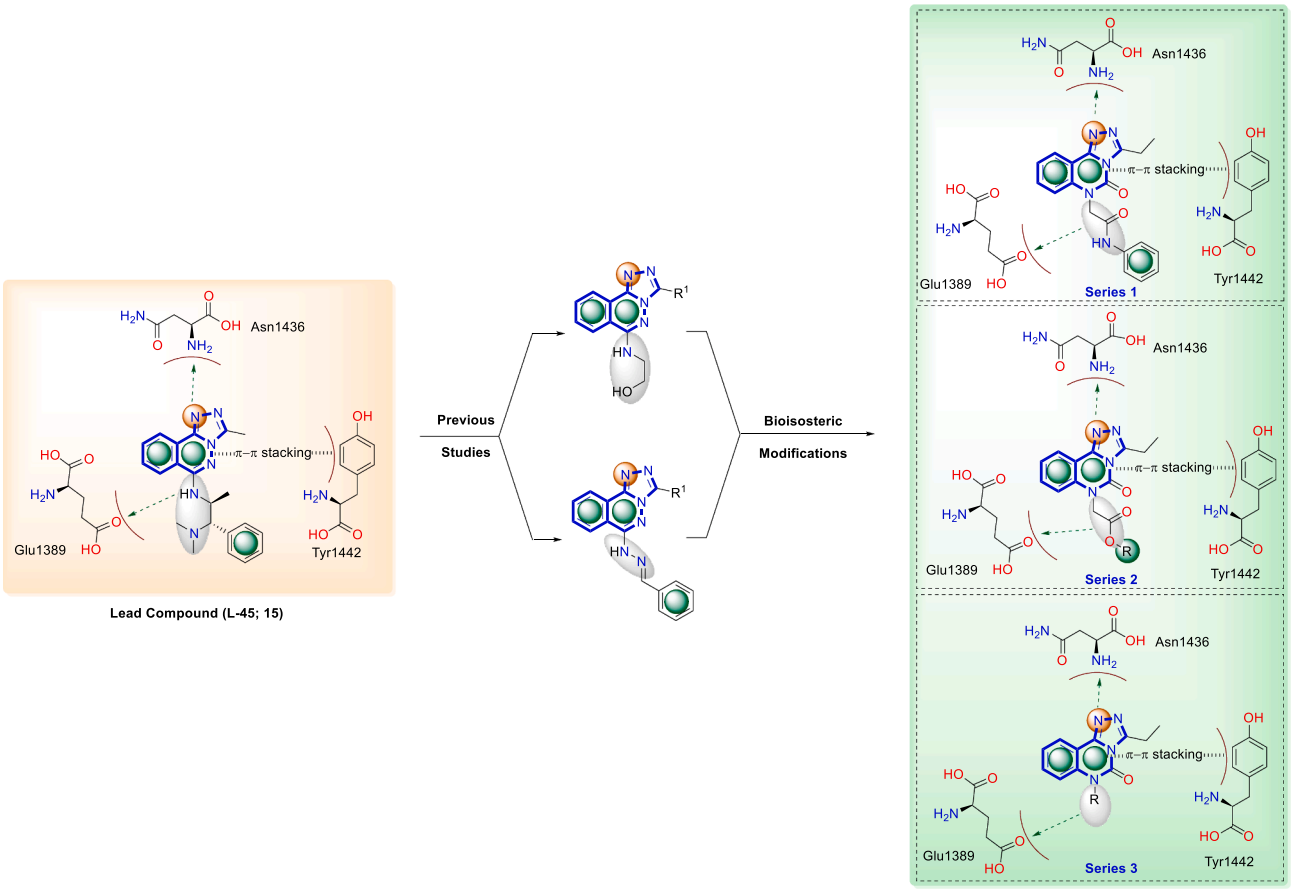

Fig. 5. Rational of molecular design of new L-45 bioisosteres as suggested PCAF inhibitors.

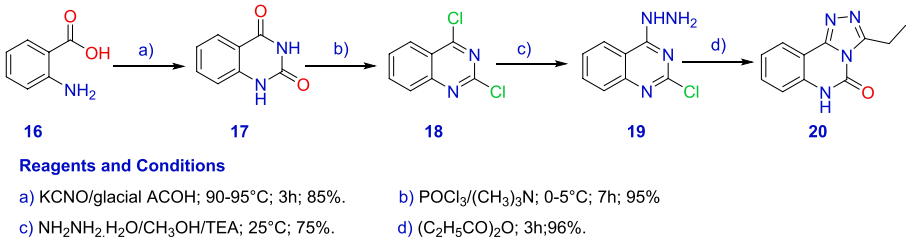

Scheme 1. Synthetic protocol of starting triazoloquinazoline.

column chromatography method.

2.2. Evaluation of biological activity

2.2.1. Cytotoxicity assay

Four cancer cell lines were selected to evaluate the cytotoxicity effects of new compounds using the MTT colorimetric assay [41]. These cells include hepatocellular, mammary gland, colorectal, and prostate carcinoma. The selection of such cancer cells depended on the overexpression of PCAF in these cell types [5,42,43]. Cytotoxicity of new ligands was compared with that of Doxorubicin as a reference anticancer agent. Results of the preliminary antiproliferative evaluation are shown in Table 1. The tabulated results showed moderate to good cytotoxicity for five of the tested compounds against selected four cancer cell lines. Concentrations of new ligands necessary for 50% inhibition of tumor cell proliferation were found to be as low as 5.75 μM. Compounds of series 1 with *N*-arylacetamide fragment at *N*-6 of the triazoloquinazoline ring system were the most effective as anticancer agents. This observation may reflect the importance of the presence of a hydrogen bond donor group at such a position to bind with the Glu1389 fragment in the target protein binding site. The electronic effect of substituents attached with the terminal phenyl ring had a remarkable impact on the cytotoxic activity of this class of compounds. Substituents with + *M* effects at C-4 of the terminal phenyl ring displayed significant inhibitory potencies with IC_{50} values ranging from 5.75 to 20.49 μM. Accordingly, the *N*-arylacetamide derivatives in series 1, compounds **22** and **24** were the most potent analogs. In particular, compound **22** showed one-third, one-half, and one-half the activity given by the reference anticancer agent against Hep-G2, MCF-7, and HCT-116 respectively. The same compound presented a more potent cytotoxicity effect against the prostate cancer cells compared with the reference drug, with an IC_{50} value of 5.75 μM. In addition, the *N*-arylacetamide derivative **24** presented remarkable cytotoxic effects against all the selected cancer cells with IC_{50} values of 20.49, 12.56, 17.18, and 11.50 μM respectively. Independently, the *para* chloro derivative **25** revealed a moderate activity with IC_{50} values of 36.59, 29.50, 43.54, and 17.65 μM against Hep-G2, MCF-7, PC3, HCT-116 respectively. Lower activities were observed for other compounds with no + *M* group attached at the *para* position of the terminal phenyl

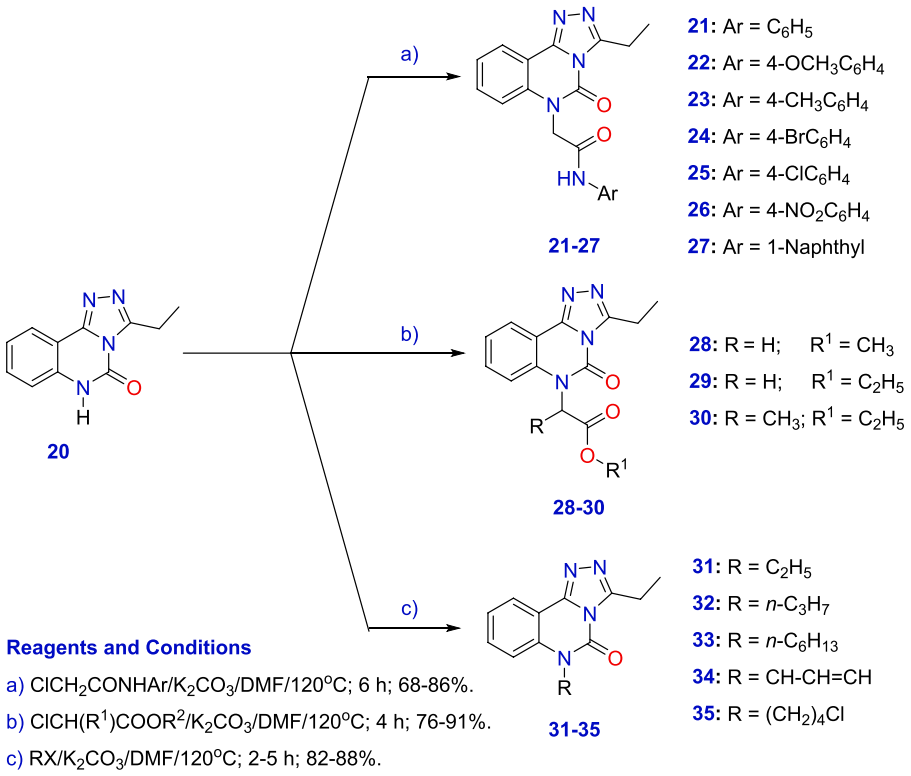

Scheme 2. Synthetic route of new triazoloquinazoline derivatives **21**–**35**.

Table 1
In vitro anticancer activity of the designed new triazoloquinazolines.

Compound #	*In vitro* Cytotoxicity IC_{50} (μM)*			
	Hep-G2	MCF-7	PC3	HCT-116
Dox**	4.50 ± 0.2	4.17 ± 0.2	8.87 ± 0.6	5.23 ± 0.3
20	33.35 ± 2.6	43.89 ± 2.8	38.62 ± 2.5	25.39 ± 2.0
21	31.51 ± 2.4	36.25 ± 2.5	29.83 ± 2.3	20.83 ± 1.8
22	15.07 ± 1.3	9.86 ± 0.8	5.75 ± 0.25	10.79 ± 1.0
23	47.36 ± 3.0	53.84 ± 3.0	57.83 ± 3.4	29.12 ± 2.5
24	36.59 ± 2.9	29.50 ± 2.5	43.54 ± 3.2	17.65 ± 1.5
25	20.49 ± 1.8	12.56 ± 1.1	17.18 ± 1.5	11.50 ± 1.0
26	64.60 ± 3.8	41.32 ± 3.0	76.37 ± 4.1	34.06 ± 2.8
27	64.13 ± 3.5	72.44 ± 3.7	69.29 ± 3.7	40.27 ± 3.2
28	44.82 ± 2.8	49.72 ± 2.9	52.46 ± 3.1	28.95 ± 2.3
29	62.79 ± 3.5	89.36 ± 4.9	79.16 ± 4.5	53.55 ± 3.9
30	81.45 ± 4.3	78.01 ± 4.2	75.14 ± 4.4	45.87 ± 3.4
31	>100	>100	>100	81.77 ± 4.6
32	84.19 ± 4.5	93.48 ± 5.3	>100	61.45 ± 4.1
33	59.23 ± 3.4	76.92 ± 4.0	74.28 ± 4.2	44.18 ± 3.3
34	78.06 ± 4.1	82.33 ± 4.5	71.30 ± 3.9	49.13 ± 3.6
35	51.40 ± 3.2	66.57 ± 3.5	63.29 ± 3.7	38.20 ± 3.0

Cancer cells treated with the test compound for 72 h and cytotoxicity expressed as the concentration needed to inhibit 50% of tumor cell proliferation (IC_{50}). Data here are presented as the means of three independent experiments ± SD.

* IC_{50} (μM): 1 – 10 (very strong). 11 – 20 (strong). 21 – 50 (moderate). 51 – 100 (weak) and above 100 (non-cytotoxic).

** DOX: Doxorubicin.

ring. Among this series of compounds, the *N*-naphthylacetamide derivative **27** presented the weakest activity as an anticancer agent with IC_{50} values above 40.00 μM. Higher doses (≥28.95 μM) of the ester derivatives in series 2 needed to Inhibit 50% of cell proliferation indicating moderate activity of these derivatives. The *N*-alkyl derivatives of series 3 were the weakest ones with IC_{50} values above 51.40 μM. In regard to the tested cancer cells, prostate cancer cells (PC3) and colorectal cancer cells (HCT-116) were found to be the most sensitive to the cytotoxic effect of new compounds followed by the breast cancer cells (MCF-7). Hepatocarcinoma cells (Hep-G2) were found to be the least sensitive to the cytotoxic effect of our target compounds as indicated by the higher IC_{50} values presented in Table 1.

2.2.2. PCAF inhibition enzyme assay

The predominant members of the p300/CBP family are appraised as universal transcriptional coactivators that play a crucial role in cell cycle regulation and apoptosis. Hence, dysfunction of PCAF is usually correlated with cancer [44]. Herein, compounds of series 1 with *N*-arylacetamide fragment at *N*-6 of the triazoloquinazoline ring system were the most effective as anticancer agents that encouraged us to select them for further biological studies to evaluate their inhibitory potentials on the PCAF enzyme. Compounds of this series have been subjected to *in vitro* PCAF fluorometric enzyme inhibition assay in comparison with bromosporine as a reference drug following the reported procedure [45,46]. The feedbacks concluded from Table 2 presented that all compounds of series 1 except **21** showed potent inhibitory activity against PCAF. Specifically, compounds **22** and **23** bearing electron-donating groups at C-4 of the terminal phenyl ring (either + M or + I respectively) exhibited excellent inhibitory activity toward PCAF with IC_{50} equal 2.88 and 8.96 μM respectively. Furthermore, compounds **25** and **26** containing

Table 2
IC_{50} of the highest potent derivatives and bromosporine (BSP) on PCAF.

Compound #	IC_{50} (μM)	SD
21	> 50	–
22	2.88	0.13
23	8.96	0.33
24	47.7	1.48
25	3.19	0.19
26	12.0	0.37
27	19.6	0.62
BSP	2.1	0.08

electron withdrawing groups at C-4 of phenyl ring (either –I or –M respectively) exerted promising PCAF inhibition activity with IC_{50} equal 3.19 and 12.00 μM, respectively. This suggested that compounds of series 1 (**21**–**27**) may exhibit their anticancer activity through binding to the active site of PCAF enzyme and disturb its action.

2.2.3. Apoptosis induction study

The induction of apoptotic cell death is a method with which an anticancer agent kills tumour cells [47]. In this work, a cytometric quantification study was performed to investigate the apoptosis and necrosis modes of PC3 cell death induced by compound **22**, the most active compound, using PI and annexin-V following the reported procedure [48]. The methodology of annexin-V/PI staining was performed in the selected cancer cells at a mixed molar concentration of 10 μM of compound **22** for 24 h. As presented in Fig. 6, the treatment of prostate cancer cells with **22** for 24 h produced an increase in the early apoptosis from 0.57% in the control sample (DMSO) to 2.21%, and a remarkable elevation in the percentage of cells in late apoptosis from 0.14% to 21.59%. These results suggested that the *N*-4-methoxyphenlacetamide derivative **22** might trigger the programmed cell death, rather than the necrotic pathway.

2.2.4. Cell cycle analysis

Tumour cell growth inhibitors are suggested to trigger an alteration in cell cycle distribution, preferentially the G2/M phase blockade [49]. Here, the mechanistic anticancer effect of compound **22** was further studied by investigating its effect on the cell cycle progression of the PC3 cell line (Figs. 7, and 8). The cell cycle of prostate cancer cells was assessed by using propidium iodide staining and flow cytometric analysis [50] after treatment with compound **22** for 24 h. Compared with that in control cells, compound **22** produced a remarkable aggregation of cells in the G2/M and Pre-G1 phases. An eighteen-folds increase in the PC3 cells percentage in the Pre-G1 phase and about four-folds increase in the percentage of cells in the G2/M phase could be indicative of apoptosis. These aggregations were accompanied by a concomitant decrease in the cell counts in the G0-G1 and S phases of the cell cycle. The Pre-G1 and G2/M phase results indicated that compound **22** induced apoptosis and arrest the cell cycle at the G2/M phase.

2.2.5. Selectivity index (SI)

One criterion for the anticancer drug to be good is that it should not affect the non-cancer cells. A molecule could consider as highly selective if it presented SI value ≥ 5. A molecule with moderate selectivity presents an SI value > 2 while low selectivity is considered if the SI is lower than 2 [51]. In this study, the selectivity index was calculated for the best effective cytotoxic derivative (**22**) by assessing its cytotoxicity against the non-cancer cells of the human microvascular endothelial cells (HMEC-1) and dividing the obtained IC_{50} value by the IC_{50} value of the same compound against PC3 cell line. Compound **22** presented an IC_{50} value of 46.30 μM against HMEC-1, which indicates the good selectivity of the new L-45 bioisostere toward the cancer cells (SI = 8.05).

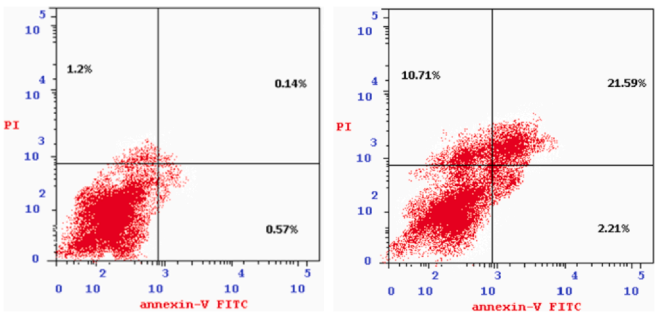

Fig. 6. Apoptotic cell death of PC3 induced by DMSO (left side) and compound **22** (right side).

2.3. Molecular docking study

In this work, a molecular docking study was conducted to give guidance of molecular binding modes of the target compounds inside the pocket of histone acetyltransferase. Docking was conducted using MOE2014 to determine the free energy and binding mode. The selection of promising molecules depended on both the perfect binding mode and the best binding free energy. With three main key interactions, the binding mode of the co-crystallized ligand, L-45 with the active site of histone acetyltransferase PCAF exhibited a binding energy of −13.16 kcal/mol. These interactions include: i) a hydrogen bond between Glu1389 residues and the dimethylamino motif of L-45; ii) a π-π stacking interaction between Tyr1442 and the pyridazine ring of the triazolophthalazine motif; iii) a hydrogen bond between the triazole ring and Asn1436 residue. An outline of free energy of bindings, H-bonding interactions, and hydrophobic interactions of the newly designed L-45 bioisosteres and that of the re-docked internal co-crystallized ligand is shown in Table 3.

The binding mode of compound **22**, as a representative example of *N*-arylacetamide derivatives bearing a substituent with + *M* effect at C-4 of the terminal phenyl ring, presented a typical binding interaction pattern with that of L-45 with the active site of the target protein. Also, the distances of hydrogen bond with the Glu1389 and π-π interactions with Tyr1442 are identical for the new triazoloquinazoline bioisostere and the co-crystallized ligand. A hydrogen bond formed between the carbonyl group of Glu1389 residue and the NH of terminal acetamide moiety in **22**. A favorable hydrophobic interaction in the form of π-π stacking has also been observed between Tyr1442 of the target protein and the pyrimidine ring of the triazoloquinazoline motif. This latter matches the hydrophobic interaction of the pyridazine ring of L-45 and the same amino acid residue. The third interaction has been revealed as a hydrogen bond between the triazole ring and the Asn1436 residue. One additional binding between **22** and PCAF receptor binding site has been found in the form of a hydrogen bond between the Glu1389 residue and the terminal acetamide moiety, in which the CH_2 fragment played as a side chain donor. These four desirable interactions may describe the good anticancer activity of this derivative.

The *N*-arylacetamide derivative with *para* bromo substituent of the terminal benzene ring (**24**), exhibited an affinity value of −10.62 kcal/mol. Obeying almost the same interaction pattern of *L*-45 with the binding site of the receptor protein, the triazole ring formed a hydrogen bond with Asn1436 residue. The pyrimidine ring interacted with Tyr1442 *via* π-π stacking while the NH of acetamide moiety at position 6 interacted *via* hydrogen bond with Glu1389 (Fig. 8 **&** Table 4). Similarly, compound **25** with *para* chloro substituent of the terminal phenyl ring revealed a similar virtual binding with the receptor target site. It exhibited an affinity value of −11.04 kcal/mol and interacted with the active site of histone acetyltransferase PCAF as following: i) a hydrogen bond is formed between the carbonyl oxygen of Glu1389 and the NH of the acetamide moiety; ii) a π-π stacking interaction between the Tyr1442 residue and the pyrimidine ring; iii) a hydrogen bond between the triazole ring of **25** and the Asn1436 residue. Following the same pattern of **22**, one more hydrogen bond is formed between the Glu1389 residue and the terminal acetamide moiety, in which the CH_2 fragment played as a side chain donor.

With much lesser binding free energies (-10.05 and −10.98), the other *N*-arylacetamide derivatives without group possessing + M effect at C-4 of the terminal phenyl ring (**21,** and **23**), showed binding modes which are also almost like that of *L*-45. The *N*-1 of the triazole rings in each compound formed a hydrogen bond with the Asn1436 residue. The pyrimidine ring formed a hydrophobic π-π stacking with Tyr1442 and the NH of the acetamide moiety interacted with Glu1389 by a hydrogen bond. Independently, compound **27**, a derivative with a bulky aryl ring attached with the acetamide fragment, exhibited a different virtual binding mode from that of *L*-45. Compound **27** revealed an affinity value of −9.07 kcal/mol and showed only two interactions with the binding

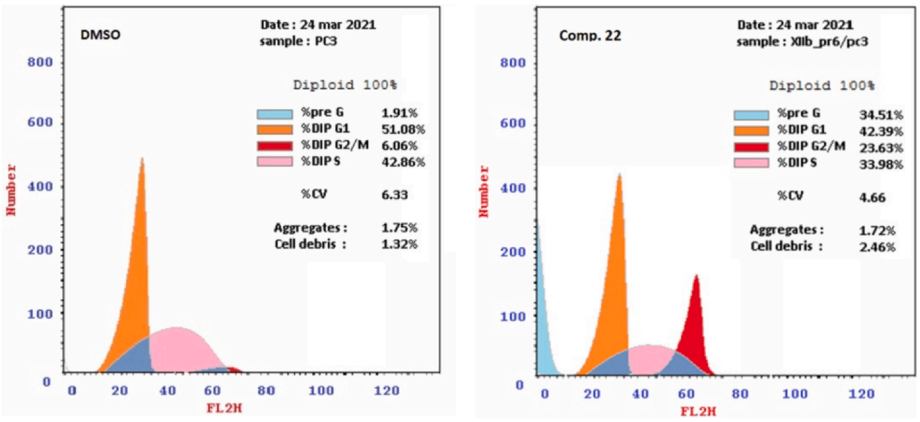

Fig. 7. Cell cycle phase distribution in PC3 cells treated with DMSO (left side) and compound **22** (right side).

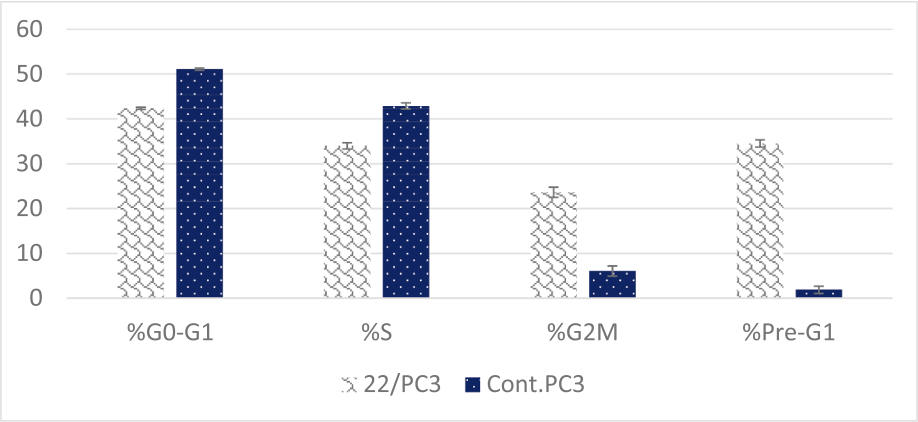

Fig. 8. Cell cycle phase distribution of PC3 cells treated with DMSO (dark bars) and compounds **22** (light bars).

site of histone acetyltransferase PCAF. These interactions involve one arene-H interaction between the pyrimidine ring of **27** with Tyr1442 and one hydrogen bond between the NH of acetamide moiety at position 6 and the Glu1389 amino acid residue. No interaction formed with the essential amino acid Asn1436, which may reflect the lower activity of such compound.

Collectively, the obtained results of molecular docking studies showed that all the designed acetamide bioisosteres of L-45 have almost similar positions and orientations inside the binding site of histone acetyltransferase PCAF (Fig. 9 **&** Table 4). As well, the distribution of binding free energies calculated from MOE software showed preferentially that the two most active derivatives; **22** and **24** are highly correlated with the biological activity, Moreover, the presence of electron-donating group with + *M* effect attached at the C-4 of terminal benzene ring excreted a good impact on binding affinity and consequently the anticancer activity. Compounds in series 2 and 3 revealed lower free energies of binding (from −6.06 to −8.55 kcal/mol) and all lack the hydrogen bond with the essential amino acid residue, Glu1389. This missing interaction may explain the lower activities of compounds in both series (Table 5).

2.4. *In silico pharmacokinetic study*

The in silico investigational study of the three most effective cytotoxic agents (**22, 24,** and **25)** was conducted (see supporting information), to evaluate their physicochemical properties based on directions of Lipinski's rule [52]. In this study, while the newly designed triazoloquinazoline bioisosteres of L-45 did not violate any of Lipinski's rules, the reference anticancer drug doxorubicin violated two rules (molecular weight and HB acceptors). All the best effective three anticancer derivatives have HB acceptor groups between 6 & 7 and only 1 HB donor, which is agreed with Lipinski's rules.

Calculation of ADMET profiles was conducted using the protocol of pkCSM descriptors algorithm [53]. From the obtained data, it could be concluded that these derivatives could show lower solubility in water (−4.163 to −3.99) compared with −2.91 and −3.03 in the case of doxorubicin and bromosporine, respectively. On the other hand, the intestinal absorptivity of newly designed triazoloquinazoline bioisosteres of L-45 in humans is expected to be relatively better than that of the reference compounds. Evaluating the volume of distribution and the CNS permeability, the new triazoloquinazoline bioisosteres are suggested to have intermediate VDs values between that of doxorubicin and bromosporine. In regard to the in silico predicted metabolism, it is noticeable that the new L-45 bioisosteres and bromosporine could inhibit the CYP3A4, the key enzyme in the metabolism of doxorubicin could not. Excretion was evaluated based on the total clearance. The obtained data revealed that **22** revealed a comparable predicted maximum total clearance value with that of doxorubicin (0.634 compared with 0.987 respectively). Dissimilar to these two compounds, **24, 25**, and bromosporine are expected to have lower total clearance values (-0.022–0.179). Thus, these latter could be excreted slower, and accordingly, they have the preference of possible longer dosing intervals. The last parameter analyzed in the pharmacokinetic profiles of our newly synthesized derivatives is their predicted toxicity. All the new triazoloquinazoline isosteres of L-45 shared the advantage of no expected AMES toxicity which indicates the preferential of probable non-mutagenic potentials of these compounds [54]. Additionally, they also suggested to not inhibit the hERG I activity, which indicates the safety of

Table 3
Results of *in silico* docking for new compounds and the co-crystallized ligand (L-45) with the binding site of histone acetyltransferase PCAF.

Comp.	ΔG (kcal/mol)	RMSD (Å)	H-bonding interactions		Hydrophobic interactions	
			Residue	Distance (Å)	Residue	Distance (Å)
L-45	−11.52	0.81	Glu1389	3.47		
			Glu1389	2.82		
			Asn1436	3.40		
					TYR 1442	3.63
21	−10.05	0.93	Glu1389	3.47		
			Glu1389	2.85		
			Asn1436	2.93		
			Tyr1442	2.93		
					TYR 1442	3.64
22	−11.31	1.18	Glu1389	3.47		
			Glu1389	2.82		
			Asn1436	3.40		
					TYR 1442	3.63
23	−10.98	1.15	Asn1436	3.16		
					TYR 1442	3.77
24	−10.62	1.16	Glu1389	3.67		
			Asn1436	3.13		
					TYR 1442	3.79
25	−11.04	0.93	Glu1389	3.47		
			Glu1389	2.82		
			Asn1436	3.40		
					TYR 1442	3.63
27	−9.07	1.20	Glu1389	2.84		
					TYR 1442	3.65
28	−8.55	1.07	Glu1389	3.40		
			Asn1436	3.34		
					VAL 1385	3.71
					TYR 1442	3.65
29	−8.43	1.20	Asn1436	3.18		
					TYR 1442	3.65
30	−6.39	1.12	Asn1436	2.99		
					TYR 1442	3.66
31	−5.25	0.93	Asn1436	2.86		
					TYR 1442	3.89
32	−6.06	1.10	Asn1436	2.99		
					TYR 1442	3.77
35	−6.50	0.61			TYR 1442	4.00
					TYR 1442	3.81

these new agents on the human' heart electrical activity [55]. unfortunately, they are expected to share the disadvantage of both reference drugs as they could inhibit the human ether-à-go-go-related gene, hERG II, which indicates the possibility of cardiac arrhythmia. As well, all the new ligands and reference drugs shared the obstacle of expected hepatotoxicity. Regarding the maximum tolerated dose in humans, the new ligands were suggested to have higher tolerability than that of doxorubicin, which means the advantage of wide therapeutic indices of the new derivative. Honorably, the newly designed bioisosteres are expected to show lower Minnow toxicity values than that of both reference compounds (-0.59, −0.35, and 0.21 compared with 4.412 and 0.952, for doxorubicin and bromosporine, respectively). These lower values of Minnow toxicities indicate lower hazards and risk of new compounds in the aquatic environment [56]. Finally, oral acute toxic doses of the new compounds (LD_{50}), are expected to be comparable or even slightly higher than that of the reference anticancer drugs (~2.75 for our new ligands compared with 2.40 and 2.1 of doxorubicin and bromosporine, respectively).

2.5. Structure-activity relationship study

As mentioned above, studying the SAR of new triazoloquinazoline bioisosteres of L-45 as anticancer agents is a major objective of the present study. Comparing the cytotoxic activity of compounds **21**–**27** incorporating an *N*-arylacetamide moiety at *N*-6 (Series 1) with that of compounds **28**–**30** incorporating ester group at the same position (Series 2), indicated that there is a marked decrease in the activity upon replacing HBD/HBA fragments with a hydrogen bond acceptor fragment. This observation may reflect the importance of the presence of a hydrogen bond donor group at such a position to bind with the Glu1389 fragment in the target protein binding site. A dramatic fall in the activity has also been observed upon attachment of an alkyl group instead of the last two fragments (Fig. 10). The electronic effect of substituents attached with the terminal phenyl ring of *N*-arylacetamide moiety had a remarkable impact on the cytotoxicity. Substituents with + *M* effects at the *para* position displayed a remarkable positive impact on the anticancer activity. Accordingly, the *N*-arylacetamide derivatives in series 1, compounds **22** and **24** were the most potent analogs. Among the *N*-arylacetamide derivatives, the bulky *N*-naphthylacetamide derivative revealed the least activity as an anticancer agent. The relative lower cytotoxic inhibitory effects of such compounds may be due to the inability of such compounds to accommodate the binding site of the target receptor.

3. Conclusion

In summary, we are here reporting the bioisosterism-guided approach for the design of three novel series of triazoloquinazolines derivatives with the objective of developing new analogous structures of the first reported PCAF inhibitor L-45. The target compounds were designed based on keeping essential structural fragments that are essential for binding with the PCAF receptor binding site with two bioisosteric modification of the lead compound: pyridazine ring of L-45 was replaced with its isosteric pyrimidine to keep the favorable π-π stacking interaction with the Tyr1442 residue; different substitution patterns were introduced to the position 6 of triazoloquinazoline scaffolds to investigate the effect on both the cytotoxic activity and binding affinities with the PCAF target protein. A follow up enzymatic assay was conducted on the best effective compounds to determine their potentials as PCAF inhibitors. Results of the PCAF enzyme assay revealed the powerful inhibitory effects of **22** and **25**. Additionally, compound **22** was selected to investigate its ability to induce apoptotic cell death and to arrest the cell cycle of PC3 cancer cells. The most active candidates in the quest for effective cytotoxic agents will serve as useful leads and merit further investigations.

4. Experimental section

4.1. General

Melting points were measured using electrothermal (Stuart SMP30) apparatus and were uncorrected. Infrared spectra were recorded on Pye

Table 4
The 3D binding interactions and the 3D positioning of co-crystallized ligand L-45, **22, 24,** and **25** with the active site of histone acetyltransferase.

Comp.	3D Interaction	3D Protein positioning
***L*-45**	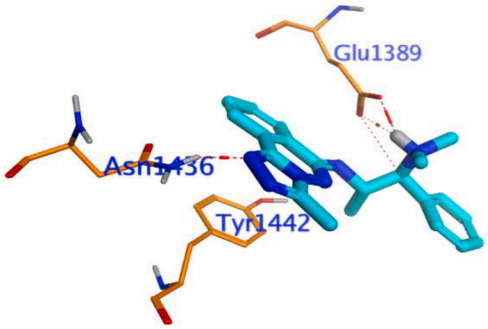	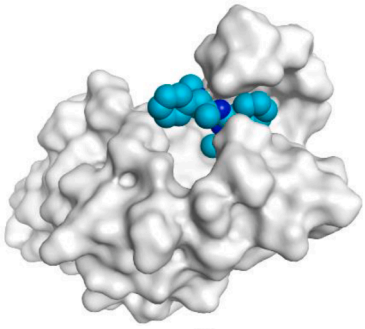
22	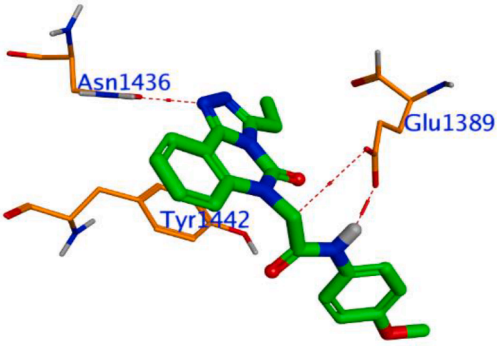	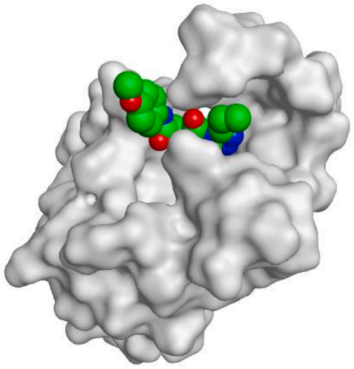
24	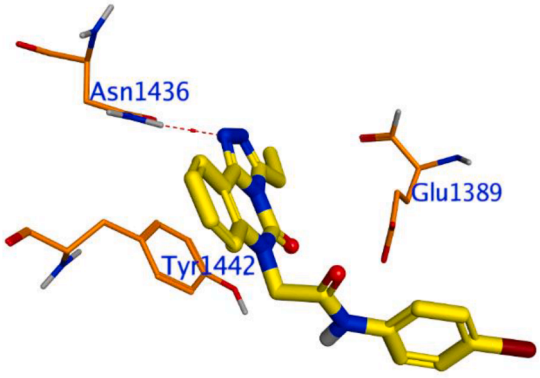	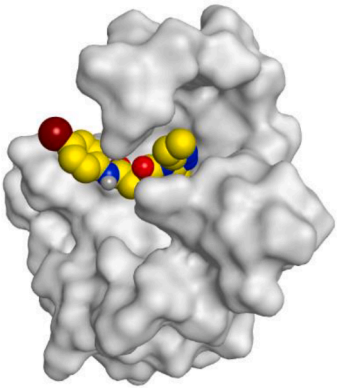
25	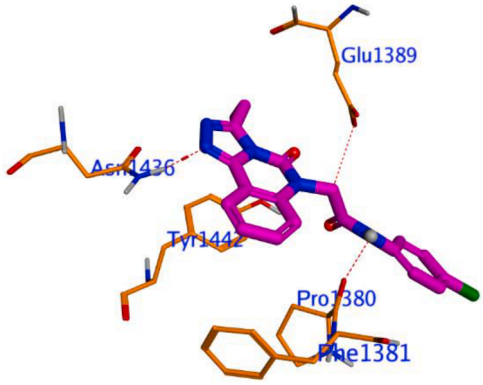	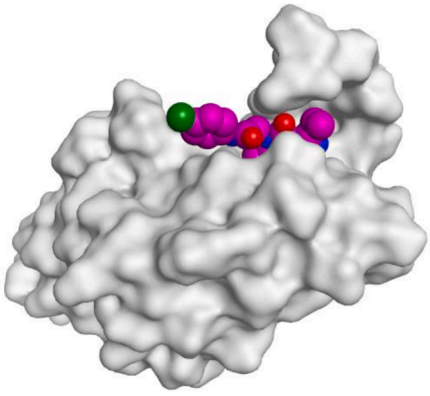

Unicam SP 1000 IR spectrophotometer at the Pharmaceutical Analytical Unit, Faculty of Pharmacy, Al-Azhar University. ^{1}H NMR and ^{13}C NMR spectra were recorded in DMSO-d_6 at 300 and 100 MHz respectively on a Varian Mercury VXR-300 NMR spectrometer at NMR Lab, Faculty of Science, Cairo University. TMS was used as an internal standard, chemical shift and coupling constant values are listed in ppm and Hz, respectively. Mass spectra and elemental analyses were carried out at the Regional Center of Mycology and Biotechnology, Al-Azhar University, Cairo, Egypt. Reaction progress were monitored with Merck silica gel IB2-F plates (0.25 mm thickness) and were visualized under a UV lamp

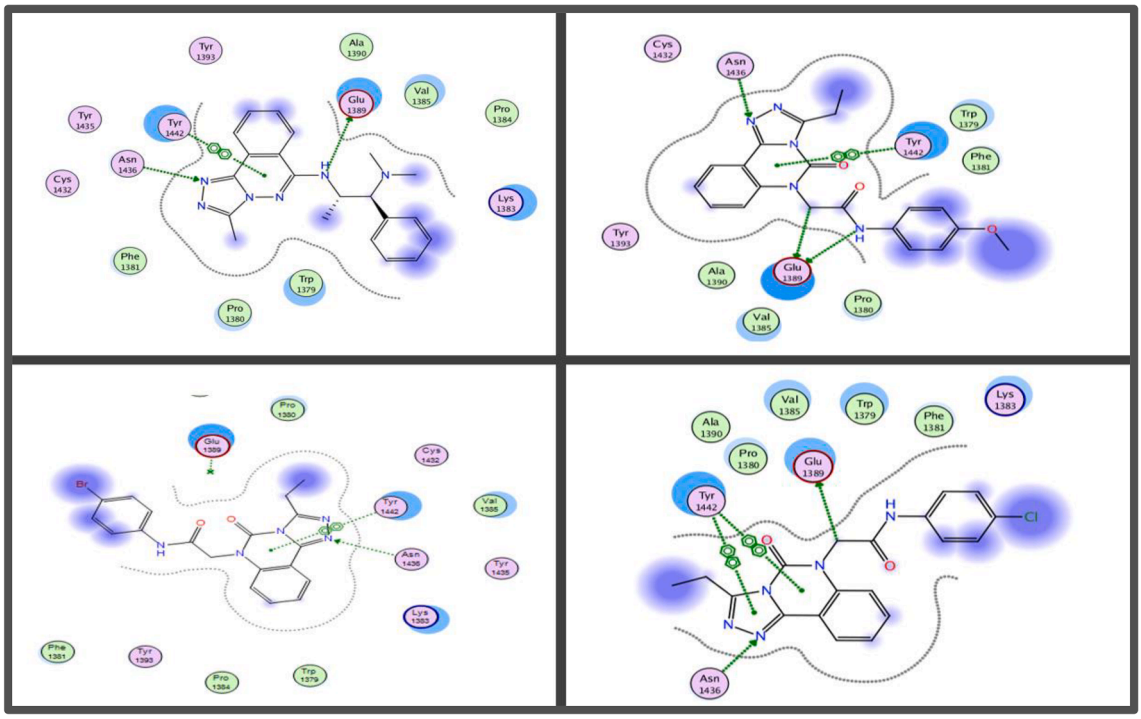

Fig. 9. 2D interactions of the co-crystallized ligand L-45 (upper left panel), **22** (upper right panel), **24** (lower left panel), and **25** (lower right panel) with the active site of histone acetyltransferase (PDB ID 5tpx).

Table 5
ADMET profile of the three most active derivatives, the reference anticancer, and PCAF inhibitor.

Parameter	22	24	25	Doxorubicin	Bromosporine
Molecular Properties					
Molecular Weight	377.404	426.274	381.823	543.525	404.452
LogP	2.2539	3.0078	2.8987	0.0013	2.34804
Rotatable Bonds	5	4	4	5	5
HB Acceptors	7	6	6	12	8
HB Donors	1	1	1	6	2
Surface Area	159.937	162.326	158.762	222.081	161.528
Absorption					
Water solubility	−3.99	−4.163	−4.106	−2.915	−3.035
Intestinal abs. (human)	97.919	95.478	95.545	62.372	82.254
Distribution					
VDss (human)	−0.155	−0.221	−0.24	1.647	−0.361
BBB permeability	−0.615	−0.586	−0.577	−1.379	−1.473
CNS permeability	−2.536	−2.224	−2.247	−4.307	−3.277
Metabolism					
CYP3A4 substrate	Yes	Yes	Yes	No	Yes
CYP3A4 inhibitor	No	Yes	Yes	No	No
Excretion					
Total Clearance	0.634	−0.179	−0.158	0.987	0.022
Toxicity					
AMES toxicity	No	No	No	No	No
Max. tolerated dose	0.156	0.115	0.113	0.081	0.606
hERG I inhibitor	No	No	No	No	No
hERG II inhibitor	Yes	Yes	Yes	Yes	Yes
Oral Rat Acute Toxicity (LD_{50})	2.738	2.751	2.75	2.408	2.148
Oral Rat Chronic Toxicity (LOAEL)	1.084	1.713	1.723	3.339	1.783
Hepatotoxicity	Yes	Yes	Yes	Yes	Yes
Minnow toxicity	−0.592	−0.358	−0.212	4.412	0.952

using different solvent systems as mobile phases. Reagents and starting anthranilic acid, phosphorus oxychloride, hydrazine hydrate, propionic anhydride, alkyl halides, alkyl-α-chloroacetate, chloroacetyl chloride, and aniline derivatives were purchased from Aldrich chemical company and were used as received. Compounds **19** and **20** were synthesized according to the directions of previously reported procedures [31].

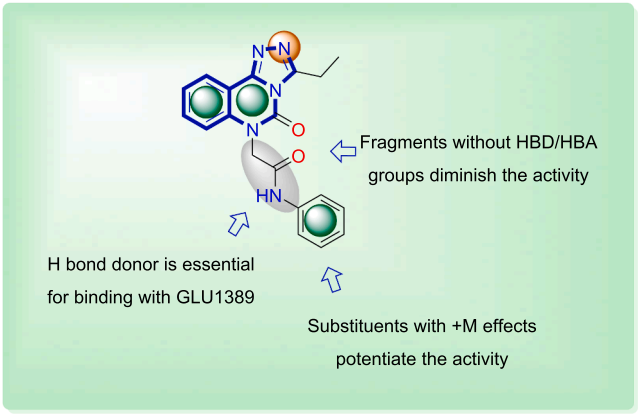

Fig. 10. Summary of SAR study of the synthesized triazoloquinazolines bioisosteres.

4.2. Synthesis of (3-ethyl -[1,2,4]triazolo[4,3-c]quinazolin-5(6H)-one (20)

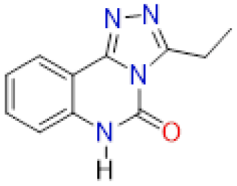

A solution of 2-chloro-4-hydrazinylquinazoline **19** (2.25 g, 0.012 mol) in propionic anhydride (15 ml) was heated under reflux for 3 h. After the reaction goes to completion (monitored by TLC), the reaction mixture was concentrated under reduced pressure. The obtained solid product was washed with three portions of *n*-hexane, 30 ml each, and dried to give the desired product as a yellowish white solid, Yield: 96%, m.p. 263–265 °C. IR (KBr) cm^{-1}: 3425 (NH), 3043 (CH aromatic), 2970 (CH aliphatic), 1755 (C═O), 1600 (C═C aromatic). ^{1}H NMR (DMSO-d_6) δ ppm: 12.28 (S, 1H, NH, D_2O exchangeable), 8.11–8.13 (d, J = 8.4 Hz, 1H, quinazoline-*H*10), 7.66–7.68 (dd, J = 7.6 Hz, 1H, quinazoline-H8), 7.39–7.41 (d, J = 8.4 Hz, 1H, quinazoline-H7), 7.35–7.37 (dd, J = 8.4 Hz, 1H, quinazoline-H9), 2.84 (q, J = 8.4 Hz, 2H, CH_2CH_3), 1.33 (t, J = 8.4 Hz, 3H, CH_2CH_3). ^{13}C NMR (DMSO-d_6) δ ppm: 167.83 (C═O), 153.16 (quinazoline-C4), 144.26 (triazole-C3), 137.39 (quinqzoline-C8a), 133.07 (quinazoline-C7), 124.48 (quinqzoline-C5), 123.99 (quinqzoline-C6), 116.50 (quinqzoline-C8), 110.65 (quinazoline-C4a), 22.04 (CH_2), and 12.57 (CH_3). MS (*m/z*): 214 ($C_{11}H_{10}N_4O$,73.34%), 213 ($C_{11}H_9N_4O$, 100%, $M^{+\cdot}$), 199 ($C_{10}H_7N_4O$, 3.46%),185 ($C_9H_5N_4O$, 2.04%). Anal. Calc. for: ($C_{11}H_{10}N_4O$) (M.W. = 214): C, 61.67; H, 4.71; N, 26.15%; Found: C, 61.89; H, 4.85; N, 25.98%.

4.3. General procedure for synthesis of 2-(3-ethyl-5-oxo-[1,2,4]triazolo [4,3-c]quinazolin-6(5H)-yl)-N-arylacetamide derivatives (21–27)

Into a stirred solution of 3-ethyl-[1,2,4]triazolo[4,3-*c*]quinazolin-5 (6*H*)-one (**20**) (2.14 g, 0.01 mol) in dry DMF (20 ml), few crystals of anhydrous K_2CO_3 were added followed by the appropriate 2-chloro-*N*-arylacetamide derivative (0.01 mol). The reaction mixture was heated to reflux temperature on a water bath for 6 h. After cooling to room temperature, the reaction mixture was poured onto ice-cooled water (100 ml) and stirred for one more hour. The formed precipitate was filtered off under vacuum and washed with a copious amount of water until the filtrate became neutral to litmus paper, washed with three repetitive portions of ice-cold water (20 ml), and then finally recrystallized from ethanol to afford the corresponding *N*-arylacetamide derivative.

4.3.1. 2-(3-Ethyl-5-oxo-[1,2,4]triazolo[4,3-c]quinazolin-6(5H)-yl)-N-phenylacetamide (21)

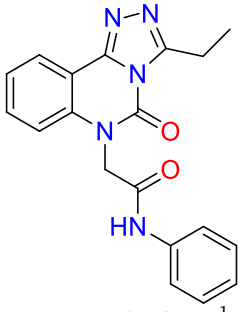

Yellowish white solid, Yield: 86%; m.p. 255–257 °C. IR (KBr) cm^{-1}: 3332 (NH), 3062 (CH aromatic), 2974 (CH aliphatic), 1693 (C═O), 1620 (C═C aromatic). ^{1}H NMR (DMSO-d_6) δ ppm: 10.43 (S, 1H, NH, D_2O exchangeable), 8.29 (d, 1H, J = 8.0 Hz, quinazoline-*H*10), 7.79 (dd, 1H, J = 7.6 Hz, quinazoline-H8), 7.60 (d,1H, J = 8.4 Hz, quinazoline-H7), 7.56 (d, 2H, J = 7.6 Hz, phenyl-H2, H6), 7.49 (dd, 1H, J = 8.4 Hz, quinazoline-H9), 7.33 (t, 2H, phenyl-H3, H5), 7.10 (t, 1H, phenyl-H4), 5.19 (S, 2H, N-CH_2), 2.90 (q, 2H, J = 8.0, CH_2CH_3), 1.36 (t, 3H, J = 8.0, CH_2-CH_3). MS (*m/z*): 347 ($C_{19}H_{17}N_5O_2$, 100%, $M^{+\cdot}$), 255 ($C_{13}H_{11}N_4O_2$, 52.04%), 227 ($C_{12}H_{11}N_4O$, 43.34%). ^{12}C NMR (DMSO-d_6) δ ppm: 168.54 (C═O), 165.50 (quinazoline-C4), 152.43 (triazole-C3), 145.10 (quinazoline-C═O), 138.85 (phenyl-C1), 138.19 (quinqzoline-C8a), 133.66 (quinazoline-C7), 129.34 (phenyl-C3, C5), 125.14 (phenyl-C4), 124.58 (quinqzoline-C5), 124.25 (quinqzoline-C6), 119.87 (phenyl-*C*2, C4), 116.11 (quinqzoline-C8), 111.22 (quinazoline-C4a), 47.32 (CH_2CO), 22.01 (CH_2), and 12.62 (CH_3). Anal. Calc. for: ($C_{19}H_{17}N_5O_2$) (M.W. = 347): C, 65.69; H, 4.93; N, 20.16%; Found: C, 65.83; H, 5.06; N, 20.40%.

4.3.2. 2-(3-Ethyl-5-oxo-[1,2,4]triazolo[4,3-c]quinazolin-6(5H)-yl)-N-(4-methoxyphenyl)acetamide (22)

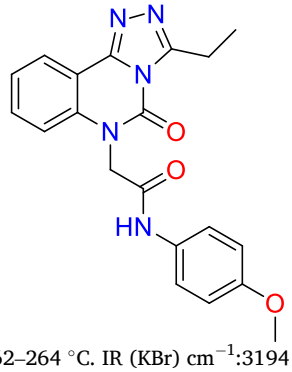

Brown solid, Yield: 75%; m.p. 262–264 °C. IR (KBr) cm^{-1}:3194 (NH), 3062 (CH aromatic), 2970 (CH aliphatic), 1674 (C═O), 1589 (C═C aromatic). ^{1}H NMR (DMSO-d_6) δ ppm: 10.05 (S, 1H, NH, D_2O exchangeable), 8.67 (d, 1H, J = 8.4 Hz, quinazoline-*H*10), 8.04 (dd, 2H, J = 8.0 Hz, phenyl-H2, H6), 7.52 (dd, 1H, J = 7.6 Hz, quinazoline-H8), 6.88 (dd, 2H, J = 8.0 Hz, phenyl-H3, H5), 6.68 (d,1H, J = 8.4 Hz, quinazoline-H7), 6.59 (dd, 1H, J = 8.0 Hz, quinazoline-H9), 4.06 (S, 2H, N-CH_2), 3.72 (S, 3H, OCH_3), 2.79 (q, 2H, J = 8.0, CH_2CH_3), 1.31 (t, 3H, J = 8.0, CH_2CH_3). ^{13}C NMR (DMSO-d_6) δ ppm: 168.33 (C═O), 161.47 (quinazoline-C4), 157.65 (triazole-C3), 155.69 (quinazoline-C═O), 146.04 (phenyl-C1), 132.47 (quinazoline-C8a), 130.21 (quinazoline-C7), 128.63 (phenyl-C3, C5 and quinazoline-C4a), 121.17 (phenyl-C4), 114.85 (quinazoline-C5), 114.48 (quinazoline-C6), 111.09 (phenyl-*C*2, C6), 111.09 (quinazoline-C8), 47.37 (CH_2CO), 21.69 (CH_3O), 19.75 (CH_2) and 11.84 (CH_3).MS (*m/z*): 377 ($C_{20}H_{19}N_5O_3$, 4.56%, $M^{+\cdot}$), 348 ($C_{18}H_{14}N_5O_3$, 1.94%). Anal. Calc. for: ($C_{20}H_{19}N_5O_3$) (M.W. = 377): C, 63.65; H, 5.07; N, 18.56%; Found: C, 63.49; H, 5.23; N, 18.72%.

4.3.3. 2-(3-Ethyl-5-oxo-[1,2,4]triazolo[4,3-c]quinazolin-6(5H)-yl)-N-(p-tolyl)acetamide (23)

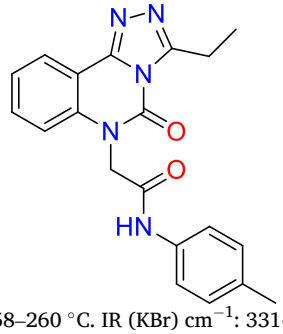

White solid, Yield: 73%; m.p. 258–260 °C. IR (KBr) cm^{-1}: 3314 (NH), 3040 (CH aromatic), 2981 (CH aliphatic), 1711 (C═O), 1518 (C═C aromatic). ^{1}H NMR (DMSO-d_6) δ ppm: 10.08 (S, 1H, NH, D_2O exchangeable), 8.09 (d, 1H, J = 8 Hz, quinazoline-*H*10), 7.95 (dd, 1H, J = 7.6 Hz, quinazoline- H8), 7.54 (dd, 2H, J = 8.0 Hz, phenyl-H2, H6), 7.48 (dd, 2H, J = 8.0 Hz, phenyl-H3, H5), 6.67 (d,1H, J = 8.4 Hz, quinazoline- H7), 6.58 (dd, 1H, J = 8.4 Hz, quinazoline- H9), 4.45 (S, 2H, N-CH_2), 2.84 (q, 2H, J = 8.0, CH_2CH_3), 2.62 (S, 1H, CH_3), 1.34 (t, 3H, J = 8.0, CH_2CH_3). ^{13}C NMR (DMSO-d_6) δ ppm: 168.58 (C═O), 158.29 (quinazoline-C4), 155.44 (triazole-C3), 146.14 (C═O), 137.62 (phenyl-C4), 136.84 (phenyl-C1), 134.31 (quinazoline-C8a), 129.74 (phenyl-C3, C5), 129.67 (quinazoline-C7), 128.44 (quinazoline-C6), 126.71 (quinazoline-C5), 119.73 (phenyl-*C*2, C6), 119.67 (quinazoline-C5), 115.91 (quinazoline-C4a), 113.90 (quinazoline-C8), 53.07 (N-CH_2), 21.13 (*p*-CH_3), 20.93 (CH_2) and 11.83 (CH_3). MS (*m/z*): 361 ($C_{20}H_{19}N_5O_2$, 1041%, $M^{+\cdot}$), 348 ($C_{19}H_{18}N_5O_2$, 15.84%), 319 ($C_{17}H_{13}N_5O_2$, 5.12%). Anal. Calc. for: ($C_{20}H_{19}N_5O_2$) (M.W. = 361): C, 66.47; H, 5.30; N, 19.38%; Found: C, 66.31; H, 5.48; N, 19.60%.

4.3.4. N-(4-Bromophenyl)-2-(3-ethyl-5-oxo-[1,2,4]triazolo[4,3-c]quinazolin-6(5H)-yl)acetamide (24)

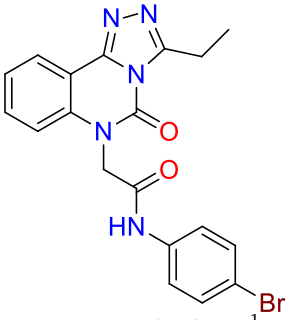

Yellowish white solid, Yield: 76%; m.p. 266–268 °C. IR (KBr) cm^{-1}: 3200 (NH), 3094 (CH aromatic), 2976 (CH aliphatic), 1661 (C═O), 1589 (C═C aromatic). ^{1}H NMR (DMSO-d_6) δ ppm: 10.32 (S, 1H, NH, D_2O exchangeable), 8.04 (d, 1H, J = 8 Hz, quinazoline-*H*10), 7.59 (dd, 2H, J = 8.0 Hz, phenyl-H2, H6) 7.50 (dd, 2H, J = 7.6 Hz, phenyl-H3, H5), 7.26 (dd, 1H, J = 7.6 Hz, quinazoline-H8), 6.70 (d,1H, J = 8.4 Hz, quinazoline-H7), 6.50 (dd, 1H, J = 8.4 Hz, quinazoline- H9), 4.11 (S, 2H, N-CH_2), 2.82 (q, J = 8.4 Hz, 2H, CH_2CH_3), 1.33 (t, J = 8.4 Hz, 3H, CH_2CH_3). ^{13}C NMR (DMSO-d_6) δ ppm: 169.13 (C═O), 161.46 (quinazoline-C4), 159.01 (triazole-C3), 157.65 (C═O), 145.98 (phenyl-C1), 138.73 (quinazoline-C8a), 137.51 (phenyl-C3, C5), 132.08 (quinazoline-C7), 128.62 (quinazoline-C6), 122.91 (quinazoline-C5), 121.55 (phenyl-C4), 117.09 (phenyl-*C*2, C6), 115.31 (quinazoline-C8), 114.53 (quinazoline-C4a), 47.47 (*N*-CH_2), 19.76 (CH_2) and 12.50 (CH_3). MS (*m/z*): 427 ($C_{19}H_{16}Br\ N_5O_2$, 6.61%, M + 2), 425 ($C_{19}H_{16}Br\ N_5O_2$, 15.79%, $M^{+\cdot}$), 255 ($C_{12}H_9N_5O_2$, 4.25%). Anal. Calc. for: ($C_{19}H_{16}\ BrN_5O_2$) (M.W. = 425): C, 53.54; H, 3.78; N, 16.43%; Found: C, 53.75; H, 3.94; N, 16.61%.

4.3.5. N-(4-Chlorophenyl)-2-(3-ethyl-5-oxo-[1,2,4]triazolo[4,3-c]quinazolin-6(5H)-yl)acetamide (25)

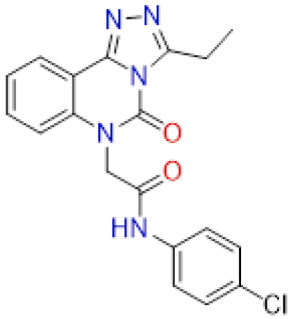

Faint greenish white solid, Yield: 78%; m.p. 253–255 °C. IR (KBr) cm^{-1}: 3294 (NH), 3094 (CH aromatic), 2925 (CH aliphatic), 1650 (C═O), 1591 (C═C aromatic). ^{1}H NMR (DMSO-d_6) δ ppm: 10.08 (S, 1H, NH, D_2O exchangeable), 8.00 (d, 1H, J = 8.0 Hz, quinazoline-*H*10), 7.56 (dd, 2H, J = 7.6 Hz, phenyl-H2, H6) 7.42 (dd, 2H, J = 8.0 Hz, phenyl-H3, H5), 7.25 (dd, 1H, J = 7.6 Hz, quinazoline-H8), 7.15 (d,1H, J = 8.4 Hz, quinazoline-H7), 6.90 (dd, 1H, J = 8.4 Hz, quinazoline-H9), 4.02 (S, 2H, N-CH_2), 2.81 (q, J = 8.4 Hz, 2H, CH_2CH_3), 1.27 (t, J = 8.4 Hz, 3H, CH_2CH_3). ^{13}C NMR (DMSO-d_6) δ ppm: 170.99 (C═O), 161.45(quinazoline-C4), 159.01 (triazole-C3), 157.56 (C═O), 145.98 (phenyl-C1), 138.72 (quinazoline-C8a), 129.18 (phenyl-C3, C5), 126.88 (quinazoline-C7), 122.56 (quinazoline-C6), 121.18 (quinazoline-C5), 120.88 (phenyl-C4), 117.07 (phenyl-*C*2, C6), 115.38 (quinazoline-C8), 114.56 (quinazoline-C4a), 57.54 (N-CH2), 19.75 (CH2), and 12.58 (CH3). MS (*m/z*): 383 ($C_{19}H_{16}ClN_5O_2$, 1.78%, M + 2), 381 ($C_{19}H_{16}Cl\ N_5O_2$, 13.51%, $M^{+\cdot}$), 352 ($C_{17}H_{11}\ ClN_5O_2$, 18.03%). Anal. Calc. for: ($C_{19}H_{16}\ ClN_5O_2$) (M.W. = 381): C, 59.77; H, 4.22; N, 18.34%; Found: C, 59.96; H, 4.37; N, 18.51.

4.3.6. 2-(3-Ethyl-5-oxo-[1,2,4]triazolo[4,3-c]quinazolin-6(5H)-yl)-N-(4-nitrophenyl)acetamide (26)

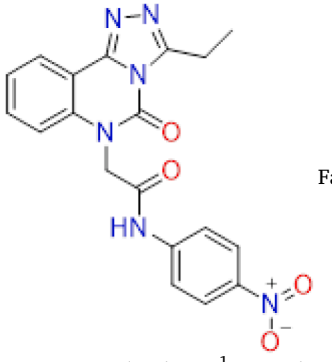

Faint brown solid, Yield: 68%; m.p. 263–265 °C. IR (KBr) cm^{-1}: 3318 (NH), 3094 (CH aromatic), 2926 (CH aliphatic), 1657 (C═O), 1583 (C═C aromatic). ^{1}H NMR (DMSO-d_6) δ ppm: 10.86 (S, 1H, NH, D_2O exchangeable), 8.28 (d, 1H, J = 8 Hz, quinazoline-*H*10), 8.04 (dd, 2H, J = 8.0 Hz, phenyl-H2, H6) 7.88 (dd, 2H, J = 8.0 Hz, phenyl-H3, H5), 7.24 (dd, 1H, J = 7.6 Hz, quinazoline-H8), 6.76 (d,1H, J = 8.4 Hz, quinazoline-H7), 6.55 (dd, 1H, J = 8.4 Hz, quinazoline-H9), 4.17 (S, 2H, N-CH_2), 2.85 (q, J = 8.4 Hz, 2H, CH_2CH_3), 1.33 (t, J = 8.4 Hz, 3H, CH_2CH_3). ^{13}C NMR (DMSO-d_6) δ ppm: 159.81 (C═O), 157.35 (quinazoline-C4), 154.12 (triazole-C3), 146.67 (C═O), 144.85 (phenyl-C4), 134.17 (phenyl-C1), 128.48 (quinazoline-C8a), 127.43 (quinazoline-C7), 126.34 (quinazoline-C6), 124.27 (quinazoline-C5), 117.81 (phenyl-C3, C5), 116.75 (phenyl-*C*2, C6), 112.12 (quinazoline-C8), 111.41 (quinazoline-C4a), 58.03 (N-CH_2), 19.26 (CH_2), and 12.17 (CH_3). MS (*m/z*): 392 ($C_{19}H_{16}N_6O_4$, 14.13%, $M^{+\cdot}$). Anal. Calc. for: ($C_{19}H_{16}\ N_6O_4$) (M.W. = 392): C, 58.16; H, 4.11; N, 21.42%; Found: C, 58.37; H, 4.25; N, 21.09%.

4.3.7. 2-(3-Ethyl-5-oxo-[1,2,4]triazolo[4,3-c]quinazolin-6(5H)-yl)-N-(naphthalen-1-yl)acetamide (27)

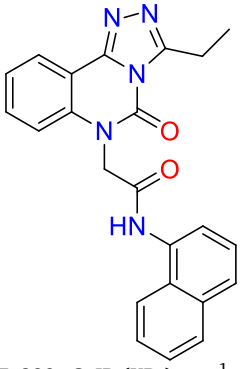

Brownish solid, Yield: 85%; m.p. 287–289 °C. IR (KBr) cm^{-1}: 3258 (NH), 3062 (CH aromatic), 2978 (CH aliphatic), 1687 (C═O), 1592 (C═C aromatic). ^{1}H NMR (DMSO-d_δ) ppm: 10.16 (S, 1H, NH, D_2O exchangeable), 8.20 (d, 2H, naphthalene-H5, H8), 7.99 (d, 2H, naphthalene-H2, H4), 7.93 (d, 1H, quinazoline-*H*10), 7.84 (d, 1H, quinazoline-H7), 7.55 (t, 3H, naphthalene- H3,H6, H7), 7.28 (dd, 1H, quinazoline-H8), 6.72 (dd, 1H, quinazoline-H9), 4.30 (S, 2H, N-CH_2), 2.79 (q, J = 8.4 Hz, 2H, CH_2CH_3), 1.29 (t, J = 8.4 Hz, 3H, CH_2CH_3). ^{13}C NMR (DMSO-d_6) δ ppm: 169.79 (C═O), 159.98 (quinazoline-C4), 157.67 (triazole-C3), 146.09 (C═O), 135.91 (naphthalene-C1), 134.18 (quinazoline-C8a), 134.16 (naphthalene-C4a), 128.97 (naphthalene-C5), 127.28 (quinazoline-C7), 126.54 (naphthalene-C3), 126.02 (naphthalene-C6), 125.80 (naphthalene-C7), 124.84 (naphthalene-C8a), 123.71 (quinazoline-C5), 123.11 (quinazoline-C6), 121.95 (naphthalene-C8), 120.40 (napthalene-C4), 115.97 (quinazoline-C8), 114.61 (quinazoline-C4a), 111.20 (naphthalene-*C*2), 47.42 (*N*-CH_2), 19.76 (CH_2), and 12.21 (CH_3). MS (*m/z*): 397 ($C_{23}H_{19}N_5O_2$, 95.72%, $M^{+\cdot}$), 255 ($C_{13}H_{11}N_4O_2$, 29.19%), 240 ($C_{12}H_8N_4O_2$, 34.04%). Anal. Calc. for: ($C_{23}H_{19}N_5O_2$) (M.W. = 397): C, 69.51; H, 4.82; N, 17.62%; Found: C, 69.75; H, 4.89; N, 17.84%.

4.4. General procedure for synthesis of alkyl 2-(3-ethyl-5-oxo-[1,2,4]triazolo[4,3-c]quinazolin-6(5H)-yl)alkanoate derivatives (28–30)

Into a stirred solution of 3-ethyl-[1,2,4]triazolo[4,3-*c*]quinazolin-5(6*H*)-one (**20**) (2.14 g, 0.01 mol) in dry DMF (20 ml), few crystals of anhydrous K_2CO_3 were added followed by the appropriate alkyl-2-chloroacetate derivative (0.01 mol). The reaction mixture was heated to reflux temperature on a water bath for 4 h. After cooling to room temperature, the reaction mixture was poured onto ice-cooled water (100 ml) and stirred for one more hour. The formed solid product was filtered off under vacuum and washed with a copious amount of water until the filtrate became neutral to litmus paper, washed with three repetitive portions of ice-cold water (20 ml), and then finally recrystallized from methanol to afford the corresponding ester derivative.

4.4.1. Methyl 2-(3-ethyl-5-oxo-[1,2,4]triazolo[4,3-c]quinazolin-6(5H)-yl)acetate (28)

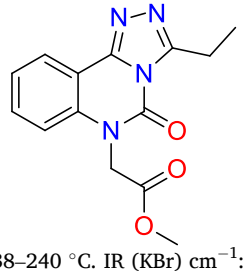

Light brown solid, Yield: 89%; m.p. 238–240 °C. IR (KBr) cm^{-1}: 3078 (CH aromatic), 2981 (CH aliphatic), 1724 (C═O), 1620 (C═C aromatic). ^{1}H NMR (DMSO-d_6) δ ppm: 8.27 (d,1H, J = 8.0 Hz, quinazoline-*H*10), 7.79 (dd, 1H, J = 7.6 Hz, quinazoline-H8), 7.63 (d,1H, J = 8.4 Hz, quinazoline-H7), 7.50 (dd, 1H, J = 8.0 Hz, quinazoline-H9), 5.21 (S, 2H, N-CH_2), 3.69 (S, 3H, OCH_3), 2.89 (q, J = 8.4 Hz, 2H, CH_2CH_3), 1.34 (t, J = 8.4 Hz, 3H, CH_2CH_3). ^{13}C NMR (DMSO-d_6) δ ppm: 168.81 (C═O), 168.70 (quinazoline-C4), 152.40 (triazole-C3), 144.85 (C═O), 137.66 (quinazoline-C8a), 133.76 (quinazoline-C7), 125.27 (quinazoline-C5), 124.82 (quinazoline-C6), 116.10 (quinazoline-C8), 111.18 (quinazoline-C4a), 53.09 (N-CH_2), 45.55 (OCH_3), 22.01 (CH_2) and 12.56 (CH_3). MS (*m/z*): 286 ($C_{14}H_{14}N_4O_3$, 100%, $M^{+\cdot}$), 227 ($C_{12}H_{11}N_4O$, 6.16%). Anal. Calc. for: ($C_{14}H_{14}N_4O_3$) (M.W. = 286): C, 58.74; H, 4.93; N, 19.57%; Found: C, 58.94; H, 5.16; N, 19.75%.

4.4.2. Ethyl 2-(3-ethyl-5-oxo-[1,2,4]triazolo[4,3-c]quinazolin-6(5H)-yl) acetate (29)

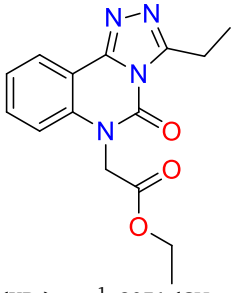

White solid, Yield: 91%; m.p. 241–242 °C. IR (KBr) cm^{-1}: 3051 (CH aromatic), 2989 (CH aliphatic), 1724 (C═O), 1620 (C═C aromatic). ^{1}H NMR (DMSO-d_6) δ ppm: 8.27 (d, 1H, J = 8.0 Hz, quinazoline-*H*10), 7.78 (dd, 1H, J = 7.6 Hz, quinazoline-H8), 7.62 (d,1H, J = 8.4 Hz, quinazoline-H7), 7.49 (dd, 1H, J = 8.0 Hz, quinazoline-H9), 5.19 (S, 2H, N-CH2), 4.19 (q, 2H, O-CH_2CH3), 2.89 (q, J = 8.4 Hz, 2H, CH_2CH_3), 1.34 (t, 3H, O-CH_2 CH_3), 1.23 (t, J = 8.4 Hz, 3H, CH_2CH_3). ^{13}C NMR (DMSO-d_6) δ ppm: 168.86 (C═O), 168.27 (quinazoline-C4), 152.36 (triazole-C3), 144.83 (quinazoline-C═O), 137.65 (quinazoline-C8a), 133.72 (quinazoline-C7), 125.24 (quinazoline-C5), 124.77 (quinazoline-C6), 116.05 (quinazoline-C8), 111.13 (quinazoline-C4a), 62.02 (OCH_2), 45.62 (N-CH_2), 22.00 (CH_2), 14.47 (CH_3) and 12.53 (CH_3).MS (*m/z*): 300 ($C_{15}H_{16}N_4O_3$, 32.27%, $M^{+\cdot}$), 271 ($C_{13}H_{11}N_4O_3$, 1.88%), 227 ($C_{12}H_{11}N_4O$, 23.86%). Anal. Calc. for: ($C_{15}H_{16}N_4O_3$) (M.W. = 300): C, 59.99; H, 5.37; N, 18.66%; Found: C, 60.15; H, 5.49; N, 18.84%.

4.4.3. Ethyl 2-(3-ethyl-5-oxo-[1,2,4]triazolo[4,3-c]quinazolin-6(5H)-yl) propanoate (30)

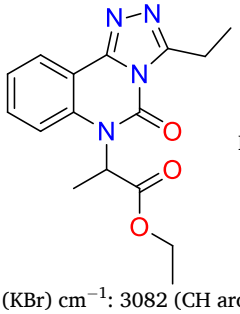

Brown solid, Yield: 76%; m.p. 246–248 °C. IR (KBr) cm^{-1}: 3082 (CH aromatic), 2981 (CH aliphatic), 1747 (C═O), 1620 (C═C aromatic). ^{1}H NMR (DMSO-d_6) δ ppm: 8.28 (d, 1H, J = 8.0 Hz, quinazoline-*H*10), 7.81 (dd, 1H, J = 7.6 Hz, quinazoline-H8), 7.80 (d,1H, J = 8.0 Hz, quinazoline-H7), 7.52 (dd, 1H, J = 8.4 Hz, quinazoline-H9), 5.80 (S, 1H, *N*-CH), 4.13 (q, 2H, OCH_2CH_3), 2.86 (q, 2H, CH_2 CH_3), 1.60 (d, 3H, J = 8.0 HzN-$CHCH_3$), 1.33 (t,3H, O-CH_2CH_3), 1.10 (t, J = 8.4 Hz, 3H, CH_2CH_3). ^{13}C NMR (DMSO-d_6) δ ppm: 169.84 (C═O), 168.57 (quinazoline-C4), 152.30 (triazole-C3), 144.04 (quinazoline-C═O), 137.29 (quinazoline-C8a), 133.29 (quinazoline-C7), 125.60 (quinazoline-C5), 124.75 (quinazoline-C6), 115.68 (quinazoline-C8), 111.54 (quinazoline-C4a), 61.62 (OCH_2), 53.52 (*N*-CH), 21.99 (CH_2), 14.54 (CH_3), 14.34 (CH_3) and 12.53 (CH_3). MS (*m/z*): 314 ($C_{16}H_{18}N_4O_3$, 100%, $M^{+\cdot}$), 285 ($C_{14}H_{13}N_4O_3$, 4.15%), 241($C_{13}H_{13}N_4O$, 3.88%). Anal. Calc. for: ($C_{16}H_{18}N_4O_3$) (M.W. = 314): C, 61.13; H, 5.77; N, 17.82%; Found: C, 61.29; H, 5.89; N, 18.04%.

4.5. General procedure for synthesis of 3-ethyl-6-alkyl-[1,2,4]triazolo [4,3-c]quinazolin-5(6H)-one derivatives (31–35)

Into a stirred solution of 3-ethyl-[1,2,4]triazolo[4,3-*c*]quinazolin-5 (6*H*)-one (**20**) (2.14 g, 0.01 mol) in dry DMF (20 ml) containing a catalytic amount of potassium iodide, few crystals of anhydrous K_2CO_3 were added followed by the appropriate alkyl halide (0.01 mol). The reaction mixture was heated to reflux temperature on a water bath for 2–5 h. After cooling to room temperature, the reaction mixture was poured onto ice-cooled water (100 ml) and stirred for one more hour. The formed solid product was filtered off under vacuum and washed with a plentiful amount of water until the filtrate became neutral to litmus paper, washed with three repetitive portions of ice-cold water (20 ml), and then finally recrystallized from methanol.

4.5.1. 3-Ethyl-6-ethyl-[1,2,4]triazolo[4,3-c]quinazolin-5(6H)-one (31)

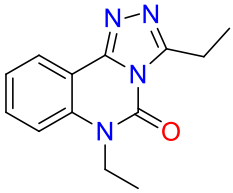

Yellowish white solid, Yield: 86%; m.p. 246–248 °C. IR (KBr) cm^{-1}: 3089 (CH aromatic), 2974 (CH aliphatic),1712 (C═O), 1642 (C═C aromatic). ^{1}H NMR (DMSO-d_6) δ ppm: 8.21–8.23 (d, J = 8.0 Hz1H, quinazoline-*H*10), 7.75–7.77 (dd, J = 7.6 Hz, 1H, quinazoline-H8), 7.70–7.72 (d, J = 8.4 Hz, 1H, quinazoline-H7), 7.42 (dd, J = 8.4 Hz, 1H, quinazoline-H9), 4.32 (q, 2H, N-CH_2), 2.82 (q, 2H, CH_2), 1.31 (t, 6H, 2CH_3). ^{13}C NMR (DMSO-d_6) δ ppm: 168.07 (quinazoline-C4), 152.15 (triazole-C3), 144.42 (quinazoline-C═O), 137.21 (quinazoline-C8a), 133.54 (quinazoline-C7), 125.19 (quinazoline-C5), 124.14 (quinazoline-C6), 116.03 (quinazoline-C8), 111.54 (quinazoline-C4a), 40.53 (N-CH_2), 22.00 (CH_2), 12.92 (CH_3) and 12.62 (CH_3). MS (*m/z*): 242 ($C_{13}H_{14}N_4O$, 100%, $M^{+\cdot}$), 213 ($C_{11}H_9N_4O$, 30.38%). Anal. Calc. for: ($C_{13}H_{14}N_4O$) (M.W. = 242): C, 64.45; H, 5.82; N, 23.13%; Found: C, 64.31; H, 5.98; N, 22.87%.

4.5.2. 3-Ethyl-6-propyl-[1,2,4]triazolo[4,3-c]quinazolin-5(6H)-one (32)

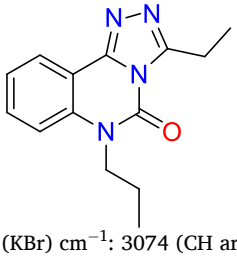

White solid, Yield: 85%; m.p. 248–250 °C. IR (KBr) cm^{-1}: 3074 (CH aromatic), 2958 (CH aliphatic),1708 (C═O), 1620 (C═C aromatic). ^{1}H NMR (DMSO-d_6) δ ppm: 8.23–8.25 (d, J = 8.0 Hz1H, quinazoline-*H*10), 7.79–7.81 (dd, J = 7.6 Hz, 1H, quinazoline-H8), 7.71–7.74 (d, J = 8.4 Hz, 1H, quinazoline-H7), 7.44 (dd, J = 8.4 Hz, 1H, quinazoline-H9), 4.26 (t, 2H, N-**CH_2**CH_2CH_3), 2.84 (q, J = 8.4 Hz, 2H, CH_2CH_3), 1.74 (m, 2H, N-CH_2 **CH_2**CH_3), 1.33 (t, 3H, N-CH_2CH_2**CH_3**), 1.00 (t, J = 8.4 Hz, 3H, CH_2CH_3). MS (*m/z*): 256 ($C_{14}H_{16}N_4O$, $M^{+\cdot}$), 213 ($C_{11}H_9N_4O$, 26.18%), 172 ($C_8H_4N_4O$, 100%). Anal. Calc. for: ($C_{14}H_{16}N_4O$) (M.W. = 256): C, 65.61; H, 6.29; N, 21.86%; Found: C, 65.39; H, 6.41; N, 22.05%.

4.5.3. 3-Ethyl-6-hexyl-[1,2,4]triazolo[4,3-c]quinazolin-5(6H)-one (33)

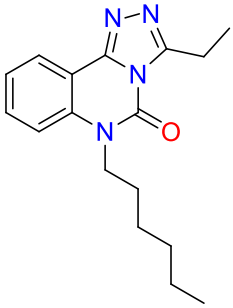

Yellow solid, Yield: 88%; m.p. 268–270 °C. IR (KBr) cm^{-1}: 3051 (CH aromatic), 2958 (CH aliphatic),1708 (C═O), 1620 (C═C aromatic). ^{1}H NMR (DMSO-d_6) δ ppm: 8.20–8.22 (d, J = 8.0 Hz1H, quinazoline-*H*10), 7.78–7.79 (dd, J = 7.6 Hz, 1H, quinazoline-H8), 7.67–7.69 (d, J = 8.4 Hz, 1H, quinazoline-H7), 7.41–7.45 (dd, J = 8.4 Hz, 1H, quinazoline-H9), 4.26 (t, 2H, N-CH_2), 2.84 (q, J = 8.4 Hz, 2H, CH_2CH_3), 1.67 (m, 2H, N-CH_2CH_2), 1.55 (t, J = 8.4 Hz, 3H, CH_2CH_3), 1.28 (m, 6H, $CH_2CH_2CH_2$), 0.86 (t, 3H, CH_3 hexyl). MS (*m/z*): 298 ($C_{17}H_{22}N_4O$, $M^{+\cdot}$), 241 ($C_{13}H_{13}N_4O$, 51.86%). Anal. Calc. for: ($C_{17}H_{22}N_4O$) (M.W. = 298): C, 68.43; H, 7.43; N, 18.78%; Found: C, 68.17; H, 7.60; N, 18.91%.

4.5.4. 6-Allyl-3-ethyl-[1,2,4]triazolo[4,3-c]quinazolin-5(6H)-one (34)

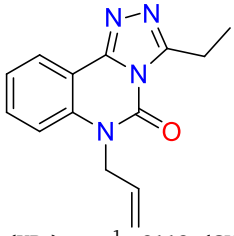

White solid, Yield: 82%; m.p. 273–275 °C. IR (KBr) cm^{-1}: 3112 (CH allyl), 3082 (CH aromatic), 2966 (CH aliphatic),1712 (C═O), 1620 (C═C aromatic). ^{1}H NMR (DMSO-d_6) δ ppm: 8.23–8.25 (d, J = 8.0 Hz1H, quinazoline-*H*10), 7.76–7.78 (dd, J = 7.6 Hz, 1H, quinazoline-H8), 7.56–7.58 (d, J = 8.4 Hz, 1H, quinazoline-H7), 7.43–7.47 (dd, J = 8.4 Hz, 1H, quinazoline-H9), 5.96 (m, 1H, CH = CH_2), 5.15–5.20 (dd, J = 10 Hz, cis, 2H, CH_2 = CH), 4.95 (d, 2H, N-CH_2), 2.87 (q, J = 8.4 Hz, 2H, CH_2CH_3), 1.36 (t, J = 8.4 Hz, 3H, CH_2CH_3). ^{13}C NMR (DMSO-d_6) δ ppm: 168.13 (quinazoline-C4), 152.35 (triazole-C3), 144.71 (quinazoline-C═O), 137.55 (quinazoline-C8a), 133.30 (allylic-CH), 132.20 (quinazoline-C7), 132.20 (quinazoline-C5), 125.04 (quinazoline-C6), 124.28 (allylic-CH), 117.38 (quinazoline-C8), 111.55 (quinazoline-C4a), 46.12 (N-CH_2), 22.02 (CH_2) and 12.60 (CH_3). MS (*m/z*): 254 ($C_{14}H_{14}N_4O$, $M^{+\cdot}$), 253 ($C_{14}H_{13}N_4O$, 100%) 213, ($C_{11}H_9N_4O$, 3.62%). Anal. Calc. for: ($C_{14}H_{14}N_4O$) (M.W. = 254): C, 66.13; H, 5.55; N, 22.03%; Found: C, 65.87; H, 5.72; N, 21.97%.

4.5.5. 6-(4-Chlorobutyl)-3-ethyl-[1,2,4]triazolo[4,3-c]quinazolin-5(6H)-one (35)

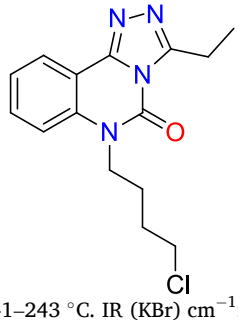

Yellowish white solid, Yield: 88%; m.p. 241–243 °C. IR (KBr) cm^{-1}: 3065 (CH aromatic), 2970 (CH aliphatic), 1693 (C═O), 1620 (C═C aromatic). ^{1}H NMR (DMSO-d_6) δ ppm: 8.23 (d, 1H, J = 8.0 Hz, quinazoline-*H*10), 7.80 (dd, 1H, J = 7.6 Hz, quinazoline-H8), 7.78 (d, 1H, J = 8.0 Hz, quinazoline-H7), 7.44 (dd, 1H, J = 8.4 Hz, quinazoline-H9), 4.34 (t, 2H, N-CH_2), 3.71 (t, 2H, CH_2 Cl), 2.85 (q, J = 8.4 Hz, 2H, CH_2CH_3), 1.88 (t, J = 8.4 Hz, 3H, CH_2CH_3), 1.3 (t, 4H, 2CH_2). MS (*m/z*): 304 ($C_{15}H_{17}ClN_4O$, 75.20%, $M^{+\cdot}$), 269 ($C_{15}H_{17}N_4O$, 16.90%), 241 ($C_{13}H_{13}N_4O$, 57.93%), 213 ($C_{11}H_9N_4O$, 51.67%). Anal. Calc. for: ($C_{15}H_{17}ClN_4O$) (M.W. = 304): C, 59.11; H, 5.62; N, 18.38%; Found: C, 59.35; H, 5.84; N, 18.50%.

4.6. In vitro cytotoxic activity

Four human cancer cell lines namely; Hepatocellular carcinoma (Hep-G2), Mammary gland breast cancer (MCF-7), Human prostate cancer (PC3), and Colorectal carcinoma (HCT-116) were obtained from VACSERA, Cairo, Egypt. Doxorubicin was used as a standard anticancer

drug for comparison. The inhibitory effects of our target compounds on cell growth of the above-mentioned cell lines were determined using the MTT assay [41].

4.7. PCAF inhibition enzyme assay

A fluorescent histone acetyltransferase estimation was applied for compounds of series 1 according to the previously reported procedure [45,58]. Three independent experiments were performed and bromosporine was used as a positive control.

4.8. Apoptosis induction study

The effects of compound **22** as an apoptosis inducer was analyzed using Annexin V-FITC/PI apoptosis detection kit. PC3 cells were stained with Annexin-V fluorescein and counterstained with propidium iodide. Then, cells in a density of $2X10^5$/well were incubated with the test compound for 48 h. Next, the cells were trypsinized, washed with phosphate-buffered saline, and finally stained for 15 min at 37 °C in the dark. FACS Caliber flow cytometer was used in the analysis process [48].

4.9. Cell cycle analysis

The effect of compound **22** on the cell cycle distribution was analyzed with a FACS Caliber flow cytometer following the reported procedures (see supporting information) [50].

4.10. Docking studies

In the present work, all docking experiments were performed for all the final target hybrid structures using Molecular Operating Environment software (MOE 2014) to evaluate the free energy of binding and to explore the binding mode toward histone acetyltransferase PCAF. Redocking of the co-crystallized ligand and docking of its newly designed final bioisosteres were performed using a default protocol against the target receptor according to the direction of our previously reported procedures [15,24].

Declaration of Competing Interest

The authors declare that they have no known competing financial interests or personal relationships that could have appeared to influence the work reported in this paper.

Acknowledgement

The authors would like to express their appreciation to Prof. Dr. Magda A. El-Sayed, Professor of Pharmaceutical Chemistry at Horus University in Egypt for her unlimited support throughout writing and revision of the article.

Appendix A. Supplementary material

Supplementary data to this article can be found online at https://doi.org/10.1016/j.bmc.2021.116266.

References

1 Brand M, Measures AM, Wilson BG, et al. Small Molecule Inhibitors of Bromodomain–Acetyl-lysine Interactions. *ACS Chem Biol*. 2015;10(1):22–39. https://doi.org/10.1021/cb500996u.
2 Muddassir M, Soni K, Sangani CB, et al. Bromodomain and BET family proteins as epigenetic targets in cancer therapy: their degradation, present drugs, and possible PROTACs. *RSC Adv*. 2021;11(2):612–636. https://doi.org/10.1039/D0RA07971E.
3 Moustakim M, Clark PGK, Hay DA, Dixon DJ, Brennan PE. Chemical probes and inhibitors of bromodomains outside the BET family. *Medchemcomm*. 2016;7(12):2246–2264. https://doi.org/10.1039/c6md00373g.
4 Moustakim M, Clark PGK, Trulli L, et al. Discovery of a PCAF Bromodomain Chemical Probe. *Angew Chemie*. 2017;129(3):845–849. https://doi.org/10.1002/ange.201610816.
5 Liu T, Wang X, Hu W, et al. Epigenetically Down-Regulated Acetyltransferase PCAF Increases the Resistance of Colorectal Cancer to 5-Fluorouracil. *Neoplasia*. 2019;21(6):557–570. https://doi.org/10.1016/j.neo.2019.03.011.
6 Tallen G, Riabowol K. Keep-ING balance: Tumor suppression by epigenetic regulation. *FEBS Lett*. 2014;588(16):2728–2742. https://doi.org/10.1016/j.febslet.2014.03.011.
7 Shagufta Ahmad I. An insight into the therapeutic potential of quinazoline derivatives as anticancer agents. *Medchemcomm*. 2017;8(5):871–885. https://doi.org/10.1039/C7MD00097A.
8 U.S. Food & Drug Adminstration. FDA approves tucatinib for patients with HER2-positive metastatic breast cancer. https://www.fda.gov/drugs/resources-information-approved-drugs/fda-approves-tucatinib-patients-her2-positive-metastatic-breast-cancer. Published 2020. Accessed February 10, 2021.
9 Mahdy HA, Ibrahim MK, Metwaly AM, et al. Design, synthesis, molecular modeling, in vivo studies and anticancer evaluation of quinazolin-4(3H)-one derivatives as potential VEGFR-2 inhibitors and apoptosis inducers. *Bioorg Chem*. 2020;94, 103422. https://doi.org/10.1016/j.bioorg.2019.103422.
10 El-Azab AS, Al-Omar MA, Abdel-Aziz AA-M, et al. Design, synthesis and biological evaluation of novel quinazoline derivatives as potential antitumor agents: Molecular docking study. *Eur J Med Chem*. 2010;45(9):4188–4198. https://doi.org/10.1016/j.ejmech.2010.06.013.
11 Al-Suwaidan IA, Abdel-Aziz AA-M, Shawer TZ, et al. Synthesis, antitumor activity and molecular docking study of some novel 3-benzyl-4(3H)quinazolinone analogues. *J Enzyme Inhib Med Chem*. 2016;31(1):78–89. https://doi.org/10.3109/14756366.2015.1004059.
12 Ezzat HG, Bayoumi AH, Sherbiny FF, et al. Design, synthesis, and molecular docking studies of new [1,2,4]triazolo[4,3-a]quinoxaline derivatives as potential A2B receptor antagonists. *Mol Divers*. 2021;25(1):291–306. https://doi.org/10.1007/s11030-020-10070-w.
13 Turky A, Sherbiny FF, Bayoumi AH, Ahmed HEA, Abulkhair HS. Novel 1,2,4-triazole derivatives: Design, synthesis, anticancer evaluation, molecular docking, and pharmacokinetic profiling studies. *Arch Pharm (Weinheim)*. 2020;353(12):2000170. https://doi.org/10.1002/ardp.202000170.
14 Turky A, Bayoumi AH, Ghiaty A, El-Azab AS, Abdel-Aziz A-MA, Abulkhair HS. Design, synthesis, and antitumor activity of novel compounds based on 1,2,4-triazolophthalazine scaffold: Apoptosis-inductive and PCAF-inhibitory effects. *Bioorg Chem*. 2020;101:104019. https://doi.org/10.1016/j.bioorg.2020.104019.
15 Turky A, Bayoumi AH, Sherbiny FF, El-Adl K, Abulkhair HS. Unravelling the anticancer potency of 1,2,4-triazole-N-arylamide hybrids through inhibition of STAT3: synthesis and in silico mechanistic studies. *Mol Divers*. 2021;25(1):403–420. https://doi.org/10.1007/s11030-020-10131-0.
16 Syed YY. Selinexor: First Global Approval. *Drugs*. 2019;79(13):1485–1494. https://doi.org/10.1007/s40265-019-01188-9.
17 Kovalenko SI. Synthesis and Anticancer Activity of 2-(Alkyl-, Alkaryl-, Aryl-, Hetaryl-)[1,2,4]triazolo[1,5-c]quinazolines. *Sci Pharm*. 2013;81(2):359–391. https://doi.org/10.3797/scipharm.1211-08.
18 Antypenko OM, Kovalenko SI, Karpenko OV, Nikitin VO, Antypenko LM. Synthesis, Anticancer, and QSAR Studies of 2-Alkyl(aryl, hetaryl)quinazolin-4(3 H)-thione's and [1,2,4]Triazolo[1,5- c]quinazoline-2-thione's Thioderivatives. *Helv Chim Acta*. 2016;99(8):621–631. https://doi.org/10.1002/hlca.201600062.
19 Driowya M, Leclercq J, Verones V, et al. Synthesis of triazoloquinazolinone based compounds as tubulin polymerization inhibitors and vascular disrupting agents. *Eur J Med Chem*. 2016;115:393–405. https://doi.org/10.1016/j.ejmech.2016.03.056.
20 Al-Salahi R, Marzouk M, Ashour AE, Alswaidan I. Synthesis and Antitumor Activity of 1,2,4-Triazolo[1,5-a]quinazolines. *Asian J Chem*. 2014;26(7):2173–2176. https://doi.org/10.14233/ajchem.2014.16849.
21 Ewes WA, Elmorsy MA, El-Messery SM, Nasr MNA. Synthesis, biological evaluation and molecular modeling study of [1,2,4]-Triazolo[4,3-c]quinazolines: New class of EGFR-TK inhibitors. *Bioorg Med Chem*. 2020;28(7), 115373. https://doi.org/10.1016/j.bmc.2020.115373.
22 Alesawy MS, Al-Karmalawy AA, Elkaeed EB, et al. Design and discovery of new 1,2,4-triazolo[4,3- c]quinazolines as potential DNA intercalators and topoisomerase II inhibitors. *Arch Pharm (Weinheim)*. November 2020. https://doi.org/10.1002/ardp.202000237.
23 Abulkhair HS, Turky A, Ghiaty A, Ahmed HEA, Bayoumi AH. Novel triazolophthalazine-hydrazone hybrids as potential PCAF inhibitors: Design, synthesis, in vitro anticancer evaluation, apoptosis, and molecular docking studies. *Bioorg Chem*. 2020;100, 103899. https://doi.org/10.1016/j.bioorg.2020.103899.
24 Patani GA, LaVoie EJ. Bioisosterism: A Rational Approach in Drug Design. *Chem Rev*. 1996;96(8):3147–3176. https://doi.org/10.1021/cr950066q.
25 Martin YC. A practitioner's perspective of the role of quantitative structure-activity analysis in medicinal chemistry. *J Med Chem*. 1981;24(3):229–237. https://doi.org/10.1021/jm00135a001.
26 El-Adl K, Ibrahim MK, Khedr F, Abulkhair HS, Eissa IH. N-Substituted-4-phenylphthalazin-1-amine derived VEGFR-2 inhibitors: Design, synthesis, molecular docking and anticancer evaluation studies. e202000219 *Arch Pharm (Weinheim)*. 2020;354(3). https://doi.org/10.1002/ardp.202000219.
27 El-Adl K, El-Helby A-GA, Sakr H, et al. Design, synthesis, molecular docking, anticancer evaluations, and in silico pharmacokinetic studies of novel 5-[(4-chloro/2,4-dichloro)benzylidene]thiazolidine-2,4-dione derivatives as VEGFR-2 inhibitors. *Arch Pharm (Weinheim)*. 2020;354(2). https://doi.org/10.1002/ardp.202000279.
28 El-Helby AA, Sakr H, Eissa IH, Abulkhair H, Al-Karmalawy AA, El-Adl K. Design, synthesis, molecular docking, and anticancer activity of benzoxazole derivatives as

VEGFR-2 inhibitors. *Arch Pharm (Weinheim)*. 2019;352(10):1900113. https://doi.org/10.1002/ardp.201900113.
29 Husseiny EM. Synthesis, cytotoxicity of some pyrazoles and pyrazolo[1,5-a] pyrimidines bearing benzothiazole moiety and investigation of their mechanism of action. *Bioorg Chem*. 2020;102, 104053. https://doi.org/10.1016/j.bioorg.2020.104053.
30 Abul-Khair H, Elmeligie S, Bayoumi A, Ghiaty A, El-Morsy A, Hassan MH. Synthesis and Evaluation of Some New (1,2,4) Triazolo(4,3-a)Quinoxalin-4(5H)-one Derivatives as AMPA Receptor Antagonists. *J Heterocycl Chem*. 2013;50(5): 1202–1208. https://doi.org/10.1002/jhet.714.
31 Hannoun MH, Hagras M, Kotb A, El-Attar A-AMM, Abulkhair HS. Synthesis and antibacterial evaluation of a novel library of 2-(thiazol-5-yl)-1,3,4-oxadiazole derivatives against methicillin-resistant Staphylococcus aureus (MRSA). *Bioorg Chem*. 2020;94, 103364. https://doi.org/10.1016/j.bioorg.2019.103364.
32 El-Shershaby M, Ghiaty A, Bayoumi AH, et al. 1,2,4-Triazolo[4,3-c]quinazolines: A bioisosterism-guided approach towards the development of novel PCAF inhibitors with potential anticancer activity. *New J Chem*. 2021. https://doi.org/10.1039/D1NJ00710F.
33 Abulkhair HS, Elmeligie S, Ghiaty A, et al. In vivo- and in silico-driven identification of novel synthetic quinoxalines as anticonvulsants and AMPA inhibitors. *Arch Pharm (Weinheim)*. 2021;354(5):2000449. https://doi.org/10.1002/ardp.202000449.
34 Omar AM, Ihmaid S, Habib E-SSE, et al. The Rational Design, Synthesis, and Antimicrobial Investigation of 2-Amino-4-Methylthiazole Analogues Inhibitors of GlcN-6-P Synthase. *Bioorg Chem*. 2020;99:103781. https://doi.org/10.1016/j.bioorg.2020.103781.
35 Omar AM, Alswah M, Ahmed HEA, et al. Antimicrobial screening and pharmacokinetic profiling of novel phenyl-[1,2,4]triazolo[4,3-a]quinoxaline analogues targeting DHFR and E. coli DNA gyrase B. Bioorg Chem. 2020;96:103656. doi:10.1016/j.bioorg.2020.103656.
36 El-Adl K, Sakr H, El-Hddad SSA, El-Helby AA, Nasser M, Abulkhair HS. Design, synthesis, docking, ADMET profile, and anticancer evaluations of novel thiazolidine-2,4-dione derivatives as VEGFR-2 inhibitors. *Arch Pharm (Weinheim)*. March 2021. https://doi.org/10.1002/ardp.202000491.
37 Ihmaid S, Ahmed HEA, Al-Sheikh Ali A, et al. Rational design, synthesis, pharmacophore modeling, and docking studies for identification of novel potent DNA-PK inhibitors. *Bioorg Chem*. 2017;72:234–247. https://doi.org/10.1016/j.bioorg.2017.04.014.
38 El-Helby A-GA, Ayyad RRA, Zayed MF, Abulkhair HS, Elkady H, El-Adl K. Design, synthesis, in silico ADMET profile and GABA-A docking of novel phthalazines as potent anticonvulsants. *Arch Pharm (Weinheim)*. 2019;352(5). https://doi.org/10.1002/ardp.201800387.
39 El-Shershaby MH, El-Gamal KM, Bayoumi AH, El-Adl K, Ahmed HEA, Abulkhair HS. Synthesis, antimicrobial evaluation, DNA gyrase inhibition, and in silico pharmacokinetic studies of novel quinoline derivatives. *Arch Pharm (Weinheim)*. 2021;354(2), 2000277. https://doi.org/10.1002/ardp.202000277.
40 Mosmann T. Rapid colorimetric assay for cellular growth and survival: application to proliferation and cytotoxicity assays. *J Immunol Methods*. 1983;65(1–2):55–63.
41 Tuo H, Zheng X, Tu K, Zhou Z, Yao Y, Liu Q. Expression of PCAF in hepatocellular carcinoma and its clinical significance. *Xi Bao Yu Fen Zi Mian Yi Xue Za Zhi*. 2013;29(3):297–300. http://www.ncbi.nlm.nih.gov/pubmed/23643089.
42 Stimson L, Rowlands MG, Newbatt YM, et al. Isothiazolones as inhibitors of PCAF and p300 histone acetyltransferase activity. *Mol Cancer Ther*. 2005;4(10):1521–1532. https://doi.org/10.1158/1535-7163.MCT-05-0135.
43 Mai A, Rotili D, Tarantino D, et al. Identification of 4-hydroxyquinolines inhibitors of p300/CBP histone acetyltransferases. *Bioorg Med Chem Lett*. 2009;19(4):1132–1135. https://doi.org/10.1016/j.bmcl.2008.12.097.
44 Castellano S, Milite C, Feoli A, et al. Identification of Structural Features of 2-Alkylidene-1,3-Dicarbonyl Derivatives that Induce Inhibition and/or Activation of Histone Acetyltransferases KAT3B/p300 and KAT2B/PCAF. *ChemMedChem*. 2015;10(1):144–157. https://doi.org/10.1002/cmdc.201402371.
45 BioVision. pCAF Inhibitor Screening Kit (Fluorometric).
46 Hassan M, Watari H, AbuAlmaaty A, Ohba Y, Sakuragi N. Apoptosis and Molecular Targeting Therapy in Cancer. *Biomed Res Int*. 2014;2014:1–23. https://doi.org/10.1155/2014/150845.
47 Vermes I, Haanen C, Steffens-Nakken H, Reutellingsperger C. A novel assay for apoptosis Flow cytometric detection of phosphatidylserine expression on early apoptotic cells using fluorescein labelled Annexin V. *J Immunol Methods*. 1995;184(1):39–51. https://doi.org/10.1016/0022-1759(95)00072-I.
48 Wang Y, Ji P, Liu J, Broaddus RR, Xue F, Zhang W. Centrosome-associated regulators of the G2/M checkpoint as targets for cancer therapy. *Mol Cancer*. 2009;8(1):8. https://doi.org/10.1186/1476-4598-8-8.
49 Kim KH, Sederstrom JM. Assaying Cell Cycle Status Using Flow Cytometry. *Curr Protoc Mol Biol*. 2015;111(1). https://doi.org/10.1002/0471142727.mb2806s111.
50 Maioral MF, Bodack C do N, Stefanes NM, et al. Cytotoxic effect of a novel naphthylchalcone against multiple cancer cells focusing on hematologic malignancies. Biochimie. 2017;140:48-57. doi:10.1016/j.biochi.2017.06.004.
51 Lipinski CA, Lombardo F, Dominy BW, Feeney PJ. Experimental and computational approaches to estimate solubility and permeability in drug discovery and development settings. *Adv Drug Deliv Rev*. 1997;23(1–3):3–25. https://doi.org/10.1016/S0169-409X(96)00423-1.
52 Pires DE V, Blundell TL, Ascher DB. pkCSM: Predicting Small-Molecule Pharmacokinetic and Toxicity Properties Using Graph-Based Signatures. *J Med Chem*. 2015;58(9):4066–4072. https://doi.org/10.1021/acs.jmedchem.5b00104.
53 Hebert A, Bishop M, Bhattacharyya D, Gleason K, Torosian S. Assessment by Ames test and comet assay of toxicity potential of polymer used to develop field-capable rapid-detection device to analyze environmental samples. *Appl Nanosci*. 2015;5(6): 763–769. https://doi.org/10.1007/s13204-014-0373-7.
54 Roy S, Mathew MK. Fluid flow modulates electrical activity in cardiac hERG potassium channels. *J Biol Chem*. 2018;293(12):4289–4303. https://doi.org/10.1074/jbc.RA117.000432.
55 Wu X, Zhang Q, Hu J. QSAR study of the acute toxicity to fathead minnow based on a large dataset. *SAR QSAR Environ Res*. 2016;27(2):147–164. https://doi.org/10.1080/1062936X.2015.1137353.
56 Proto MC, Fiore D, Piscopo C, et al. Inhibition of Wnt/β-Catenin pathway and Histone acetyltransferase activity by Rimonabant: a therapeutic target for colon cancer. *Sci Rep*. 2017;7(1):11678. https://doi.org/10.1038/s41598-017-11688-x.